

# RAMiT: Reciprocal Attention Mixing Transformer for Lightweight Image Restoration

Haram Choi<sup>1</sup> Cheolwoong Na<sup>1</sup> Jihyeon Oh<sup>1</sup>  
 Seungjae Lee<sup>1</sup> Jinseop Kim<sup>1</sup> Subeen Choe<sup>1</sup>  
 Jeongmin Lee<sup>2</sup> Taehoon Kim<sup>3</sup> Jihoon Yang<sup>1\*</sup>

<sup>1</sup>Machine Learning Research Lab., Sogang University <sup>2</sup>LG Innotek <sup>3</sup>LG AI Research

## Abstract

Although many recent works have made advancements in the image restoration (IR) field, they often suffer from an excessive number of parameters. Another issue is that most Transformer-based IR methods focus only on either local or global features, leading to limited receptive fields or deficient parameter issues. To address these problems, we propose a lightweight IR network, Reciprocal Attention Mixing Transformer (RAMiT). It employs our proposed dimensional reciprocal attention mixing Transformer (D-RAMiT) blocks, which compute bi-dimensional (spatial and channel) self-attentions in parallel with different numbers of multi-heads. The bi-dimensional attentions help each other to complement their counterpart's drawbacks and are then mixed. Additionally, we introduce a hierarchical reciprocal attention mixing (H-RAMi) layer that compensates for pixel-level information losses and utilizes semantic information while maintaining an efficient hierarchical structure. Furthermore, we revisit and modify MobileNet V1 & V2 to attach efficient convolutions to our proposed components. The experimental results demonstrate that RAMiT achieves state-of-the-art performance on multiple lightweight IR tasks, including super-resolution, color denoising, grayscale denoising, low-light enhancement, and deraining. Codes will be available soon.

## 1 Introduction

Lightweight image restoration (IR) or enhancement techniques are essential for addressing inherent flaws in images captured in the wild, especially those taken by devices with low computational power. These techniques aim to reconstruct high-quality images from their distorted low-quality counterparts. However, many lightweight IR tasks with the popular vision Transformer [21] based methods remain relatively unexplored. Although many recent Transformer [92] networks have improved the IR domain [7, 110, 101, 10, 116], they are infeasible for real-world applications due to their large number of parameters. Furthermore, even the state-of-the-art lightweight IR networks consume intensive computational costs [56, 67, 123, 5, 11]. Another problem is that some IR models mainly focus on expanding the receptive field with respect to locality [56, 101, 123, 10, 11], which is insufficient to capture the global dependency in an image. This is critical because the IR networks need to refer to repeated patterns and textures distributed throughout the image [28, 67]. Meanwhile, others have tried to enlarge the receptive field globally [110, 116, 5] but have overlooked important local (spatial) information, which is conventionally essential for recovery tasks [31, 101, 10, 11]. Fig. 1 visualizes a few examples in which a successful IR depends on the ability to consider both local and global features in a given distorted low-quality image, emphasizing how significant the problem is.

\*Corresponding author.

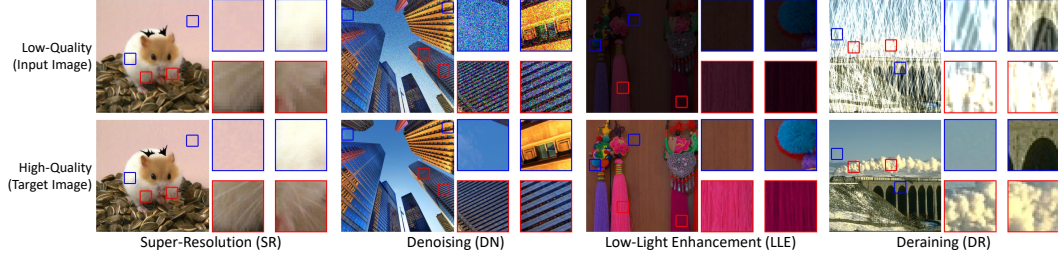


Figure 1: The importance of locality and global dependency in image restoration tasks. **(Blue boxes)** Local features are informative enough to recover most parts, meaning that the contribution of locally adjacent pixels is crucial. **(Red boxes)** Some areas seem more challenging due to high levels of distortion (blurring, noise, darkness, or obstruction). They require global dependency, which can often be detected in repeated patterns or textures distributed throughout the entire image.

To address these problems, we propose a lightweight IR network called **RAMiT (Reciprocal Attention Mixing Transformer)**. As shown in Fig. 2a, RAMiT consists of a shallow module, three hierarchical and the last stages composed of  $\mathbb{K}_a$  D-RAMiT blocks before and after an upsampling bottleneck layer, an H-RAMi, and a final reconstruction module. Our proposed **D-RAMiT (Dimensional Reciprocal Attention Mixing Transformer)** blocks include a novel bi-dimensional self-attention (SA) mixing module. This operates spatial and channel SA mechanisms [56, 110] in parallel with different multi-heads, which are then mixed. To overcome the drawbacks of each SA, we allow the results from the previous block to help the respective counterparts’ SA procedures for some tasks. Consequently, RAMiT can capture both local and global dependencies. Additionally, we propose an efficient component, **H-RAMi (Hierarchical Reciprocal Attention Mixer)** that mixes the multi-scale attentions resulting from four hierarchical stages. This component complements pixel-level information losses caused by downsampled features, and enhances semantic-level representations. It enables RAMiT to re-think where and how much attention to pay in the given input feature maps. For a mixture of each reciprocal (*i.e.*, dimensionally and hierarchically) attention result, we modify MobileNet V1 & V2 [38, 83]. Utilizing these **MobiVari (MobileNet Variant)** layers, we can efficiently and effectively attach the convolutions to the components of RAMiT.

The experimental results demonstrate that the various lightweight IR works are improved by our RAMiT-1 and RAMiT, which employ our modified versions of MobileNet V1 and V2, respectively. As a result, we establish state-of-the-art performance on five different lightweight IR tasks, including super-resolution, color denoising, grayscale denoising, low-light enhancement, and deraining, showing applicability of RAMiT to general low-level vision tasks. Notably, RAMiT achieves these results with fewer operations or parameters than the latest networks. Moreover, we provide explainable and comprehensive figures and descriptions for our proposed elements in Secs. 3.2 and 3.3.

The summaries of our main contributions are as follows:

- (1) We propose a novel dimensional reciprocal attention mixing Transformer (**D-RAMiT**) block. The spatial and channel self-attentions operate in parallel using the different numbers of multi-heads. As the proposed method mixes the bi-dimensional attentions, our RAMiT can capture both local and global context, which is critical for image restoration tasks.
- (2) A hierarchical reciprocal attention mixing (**H-RAMi**) layer is introduced. It compensates for pixel-level information losses caused by downsampled features of hierarchical structure, and utilizes semantic-level information, while maintaining an efficient hierarchical structure.
- (3) Our RAMiT achieves **state-of-the-art** results on five different lightweight image restoration tasks, including super-resolution, color denoising, grayscale denoising, low-light enhancement, and deraining. RAMiT requires fewer parameters or operations compared to existing methods.

## 2 Related Work

**Window Self-Attention.** After Vision Transformer (ViT) [21] appeared, Swin Transformer [66] proposed window self-attention (WSA) to solve the excessive time complexity of ViT. Self-attention is computed with the tokens in a non-overlapping local window. However, since the receptive field of WSA was limited within a small window despite a window shift operation, some following high-level vision studies tried to overcome this issue. GGViT [109], CrossFormer [98], and MaxViT [91]

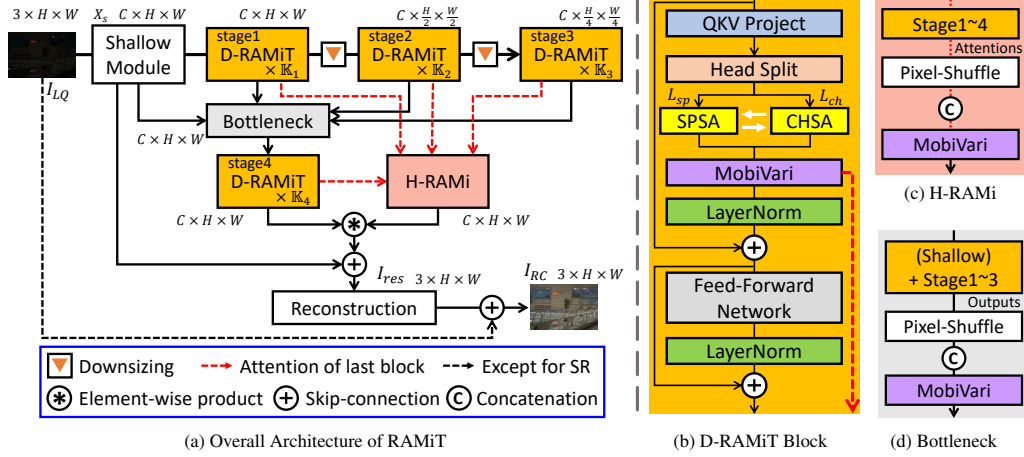


Figure 2: Overall architecture of RAMiT. **(a)** The size indicates dimension of output from each component. The operation of  $I_{LQ} + I_{res}$  is omitted for super-resolution tasks.  $I_{RC}$  equals to  $I_{res} \in \mathbb{R}^{3 \times rH \times rW}$  ( $r$ : an upscale factor). **(b)** The different multi-heads ( $L_{sp}$ ,  $L_{ch}$ ) are assigned to each self-attention (SA) module. Being multiplied to *value* of each counterpart, both SAs help each other (white arrows, optional depending on tasks). The bi-dimensional attentions are mixed by our MobileNet variant, MobiVari<sup>1</sup>. **(c)** H-RAMi mixes the hierarchical attentions resulting from the last blocks of each stage. Before MobiVari enhances and mixes the attentions, this module upsamples and concatenates multi-scale attentions. **(d)** Our bottleneck adopts the SCDP bottleneck of NGswin [11].

utilized dilated windows to capture the dependency in non-local regions. Focal Transformer [105] gradually widened surrounding regions (*key*, *value*) of a local window (*query*). CSwin[20] extended square windows to cross-shaped rectangle windows. VSA [122] dynamically varied the window size, breaking the local constraint. DaViT [16] alternately placed spatial WSA and channel self-attention blocks to consider both local and global dependencies in an image.

**WSA for Image Restoration.** The image restoration (IR) tasks aim to recover a high-quality image from a degraded low-quality counterpart. SwinIR [56] firstly adapted window self-attention (WSA) in this domain and achieved outstanding results. Thereafter, many studies employed WSA and overcame the limited receptive field. Uformer [101] proposed locally-enhanced feed-forward network to refer to neighbor pixels. ELAN [123] split channels of input feature maps into different sized windows, efficiently enlarging the local receptive field. CAT [10] used rectangle windows that were larger than the plain square windows inspired by CSwin. Following [109, 98, 91], ART [116] exploited the dilated window attention. NGswin [11] introduced an N-Gram method helping WSA to consider surrounding pattern and texture. Moreover, Restormer [110] and NAFNet [8] utilized channel-attention rather than spatial WSA for maximizing the capability of attention mechanism in capturing global dependency. Related to the approaches above, we aim to address the weakness of the plain WSA. More related works are covered in Appendix Sec. A.9.

### 3 Methodology

#### 3.1 Overall Architecture of Reciprocal Attention Mixing Transformer (RAMiT)

As shown in Fig. 2a, given a low-quality image  $I_{LQ} \in \mathbb{R}^{3(\text{or}1) \times H \times W}$ , a  $3 \times 3$  convolutional **shallow module** produces  $X_s \in \mathbb{R}^{C \times H \times W}$ , where  $H$  and  $W$  are height and width of  $I_{LQ}$ , and  $C$  is channel.  $X_s$  passes through hierarchical **encoder stages** consisting of  $\mathbb{K}_a$  **D-RAMiT** (Dimensional Reciprocal Attention Mixing Transformer, Sec. 3.2 and Fig. 2b) blocks, where  $a$  indicates the stage number. D-RAMiT calculates self-attention (SA) in bi-dimensions (spatiality and channel) with the different numbers of multi-heads. After projecting *query*, *key*, *value* and splitting current feature map into  $L$  heads,  $L_{sp}$  and  $L_{ch}(= L - L_{sp})$  heads are assigned to spatial and channel self-attention modules, respectively. For both SAs, we employ scaled-cosine attention and post-normalization [65]. The reciprocally computed attentions are mixed by **MobiVari<sup>1</sup>** (MobileNet Variants). Afterwards, the

<sup>1</sup>MobiVari modifies the activation function and residual connections [33] of the original MobileNet V1 & V2 [38, 83], and the expansion convolution of [83]. We detail the MobiVari structure in Appendix Sec. A.1.

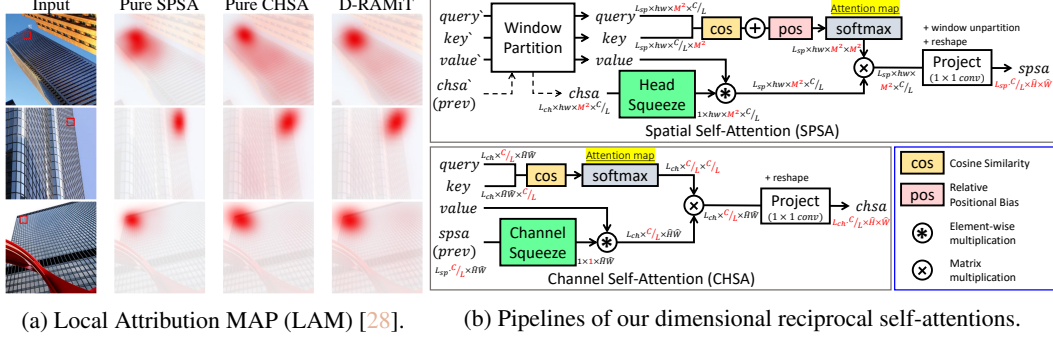


Figure 3: **(a)** The depth of the red areas indicates the extent to which the regions contribute to recovering a red box of an input. D-RAMiT utilizes both local and global dependencies, meaningfully expanding the receptive field compared to the pure SPSA (see Appendix Sec. A.3). **(b)** Our bi-dimensional self-attention schemes help each other to further boost image restoration performances.

output passes through layer-norm (LN) [4] with skip connection [33], feed-forward network, and LN. At the end of the first and second stages, we downsample the feature maps by half, but maintain the channels. While the **downsizing layers** follow the patch-merging practice of Swin Transformers [66], we replace a plain linear projection of these layers with our MobiVari.

When the stage3 ends,  $X_s$  and multi-scale outputs from stage 1, 2, 3 are fed into a **bottleneck layer** (Fig. 2d), which is the same as SCDP bottleneck from NGswin [11] except that depth- and point-wise convolution switches over to our MobiVari. The bottleneck taking multi-scale features can compensate for information loss caused by the downsizing layers. Using a bottleneck output, the **stage4** composed of  $\mathbb{K}_4$  D-RAMiT blocks operates in the same way as the other stages. Then, the merged attention results outputted by the last Transformer blocks of all the stages are conveyed to an **H-RAMi** layer (**H**ierarchical **R**eciprocal **A**ttention **M**ixer, Sec. 3.3 and Fig. 2c). H-RAMi upsamples them into  $H \times W$  using a pixel-shuffler [85] and aggregates them, which is merged by MobiVari. This layer is simple but robust to pixel-level information losses as is our bottleneck. The re-mixed hierarchical attention is element-wise multiplied to the stage4 output. A global skip-connection adds the result with  $X_s$  [47], which is then fed into the **reconstruction module** to produce a residual image  $I_{res}$ . The reconstruction module follows the common practice [2, 56, 11], but places two MobiVari layers before the original version to boost the performances (detailed in Appendix Sec. A.1). Finally,  $I_{res} + I_{LQ}$  makes a reconstructed image  $I_{RC}$  (ignored for super-resolution, *i.e.*,  $I_{res} = I_{RC}$ ).

### 3.2 Dimensional Reciprocal Attention Mixing Transformer (D-RAMiT) Block

**Motivation.** To improve low-level vision tasks like image restoration (IR), it is crucial to refer to repeated patterns and textures distributed through an entire image (*i.e.*, global or non-local context) [28, 67], as already presented in Fig. 1. Nevertheless, while many approaches for high-level vision tasks, such as classification, have enriched non-locality [109, 98, 91, 16], most lightweight IR methods lack the capability to capture global dependency. They maximize only “locality” by adding correlation of adjacent neighbors to a local window [11], or splitting the channels into three groups and the corresponding sizes of local windows within which the self-attention is computed [123]. Meanwhile, channel-attention mechanism is theoretically capable of equipping global dependency by involving all pixels along the channel dimension [39, 125, 110, 8]. Fig. 3a visualizes the actual receptive field of different self-attention methods using the Local Attribution Map [28]. The channel self-attention (**CHSA**) views nearly global areas but performs poorly (Tab 5a), because lightweight CHSA focuses on the unnecessary parts with deficient trainable parameters [12]. On the other hand, the spatial self-attention (**SPSA**<sup>2</sup>) suffers from the limited receptive field despite intensive computational costs (Tab 5a), which suggests the potential for further improvement. Hence, our goal is to incorporate local and global context rather than merely enlarging “local” receptive field.

**Proposed Method.** We propose a bi-dimensional reciprocal self-attention, which is implemented by operating both SPSA and CHSA in parallel (Fig. 2b). Our proposed method can capture both local and global range dependency, thereby improving the IR performances. As illustrated in Fig. 3b, our

<sup>2</sup>In this paper, SPSA indicates the local window-based self-attention proposed by Swin Transformer [66].



SPSA and CHSA pipelines adapt the local window self-attention of SwinIR [56] and the transposed attention of Restormer [110], respectively. We assign the different numbers of multi-heads  $L_{sp}$  and  $L_{ch}$  ( $L_{sp} + L_{ch} = L$ ) to SPSA and CHSA to compute reciprocal attention  $Attn$ , as follows:

$$\begin{aligned}
Attn &= \text{MobiVari}(\text{Concat}[SPSA, CHSA]), \text{ where} \\
SPSA &= \mathcal{P}_{sp}(\text{Concat}[head_1^{sp}, \dots, head_{L_{sp}}^{sp}]), CHSA = \mathcal{P}_{ch}(\text{Concat}[head_{L_{sp}+1}^{ch}, \dots, head_L^{ch}]), \\
head_i^{sp} &= \text{Softmax}(\cos(Q_i^{sp}, (K_i^{sp})^T) / \tau + B) V_i^{sp}, B \in \mathbb{R}^{M^2 \times M^2} \\
head_i^{ch} &= \text{Softmax}(\cos(Q_i^{ch}, (K_i^{ch})^T) / \tau) V_i^{ch},
\end{aligned} \tag{1}$$

where  $Q_i^{sp}, K_i^{sp}, V_i^{sp} \in \mathbb{R}^{h \times w \times M^2 \times C/L}$  and  $Q_i^{ch}, K_i^{ch}, V_i^{ch} \in \mathbb{R}^{C/L \times \hat{H} \times \hat{W}}$  are *query, key, value* for SPSA and CHSA, respectively;  $h$  and  $w$  indicate the number of windows at height and width of the current feature map (size of  $\hat{H} \times \hat{W}$ );  $M$  is window size and  $C/L$  equals to channels per head;  $\cos$  calculates cosine similarity [65];  $B$  is the relative positional bias [66];  $\tau$  is a trainable scalar that is set larger than 0.01 [65];  $\mathcal{P}_{sp}, \mathcal{P}_{ch}$  denotes the reshape and projection layer. Similar to our work, DaViT [16] has sequentially placed the same numbers of SPSA and CHSA blocks, improving high-level vision. However, this simple method can consider global context only after attending to spatial dimension (see Appendix Sec. A.2). In contrast, D-RAMiT processes both SAs in parallel (precisely in the same block), allocating more heads to SPSA (e.g.,  $L_{sp}:L_{ch}=75\%:25\%$ ). Then, our MobiVari mixes local and global attentions as well as enhances locality by  $3 \times 3$  depth-wise convolution [110, 101]. The subsequent process follows Fig. 2b.

**Reciprocal Helper.** Our bi-dimensional modules help each other to compensate for each others' weaknesses, thereby further boosting lightweight IR performances (optional depending on tasks). When operating SPSA of  $\ell$ -th block, *value* is element-wise multiplied with the CHSA output of  $(\ell - 1)$ -th block, before multiplying attention map<sup>3</sup> and *value*. The inverse process applies to CHSA as well. It is noteworthy that intensities of information on each SA differ. Each single channel from the previous CHSA has various global representations. Thus, we squeeze (average-pool) it at head dimension before product. On the other hand, averaging channels of SPSA can preserve valuable local properties. As a result, we squeeze feature of the previous SPSA at channel dimension. The first D-RAMiT block of each stage excludes this step due to absence of the previous features with a same resolution. We verify the effects of this approach in Tab. 5b.

**Efficiency.** The pure SPSA module employed by other IR networks [56, 123, 11] have quadratic time complexity to a local window size. On the other hand, the time complexity of a CHSA module is usually lower than that of an SPSA, as channels per head ( $C/L$ ) is mostly not larger than a local window area ( $M^2$ ) in the equations of Tab. 1. Our proposed D-RAMiT, thus, is more efficient than the pure SPSA. Mult-Adds is evaluated on a  $1280 \times 720$  high resolution (quality) image.

Table 1: **(Eq.)** Time complexity. **(Tab.)** Mult-Adds / #Parameters.

$$\begin{aligned}
\Omega(SPSA) &= 4\hat{H}\hat{W}C^2 + 2M^2\hat{H}\hat{W}C \\
\Omega(CHSA) &= 4\hat{H}\hat{W}C^2 + 2\hat{H}\hat{W}C^2/L
\end{aligned}$$

Task	Pure SPSA	D-RAMiT (proposed)
SR $\times 2$	173.4G / 975K	163.4G / 940K
SR $\times 3$	81.9G / 984K	77.3G / 949K
SR $\times 4$	44.6G / 996K	42.1G / 961K
Denoising	659.9G / 970K	620.8G / 935K

\*SR: Super-Resolution

\*Both methods have the same number of layers and channels.

### 3.3 Hierarchical Reciprocal Attention Mixer (H-RAMi)

**Motivation.** There are many evidences that a hierarchical network is usually less effective for IR tasks [11, 12, 37, 130]. This is because the goal of IR is to predict pixel values one by one (i.e., dense prediction) inferring recovery patterns when given the distribution of other pixels [28]. However, downsizing feature maps significantly loses important pixel-level information, which prevents many IR researchers from employing hierarchical structures regardless of CNN or Transformer based models [125, 2, 79, 68, 56, 123, 5]. Nevertheless, a hierarchical architecture has several advantages. First, reducing the feature map size can lower time complexity. For example, non-hierarchical SwinIR-light [56] requires intensive computations (See Tab. 2). Furthermore, a hierarchical structure can learn semantic-level feature representation as well as pixel-level [30, 97]. To complement the demerits and leverage the merits, we propose the Hierarchical Reciprocal Attention Mixing layer.

**Proposed Method.** As presented in Fig. 2c, our H-RAMi layer is simple but effective. Inspired by SCDP bottleneck [11], we apply the same strategy to “multi-scale attentions” from the hierarchical encoder stages instead of the final outputs. H-RAMi takes the attentions merged by MobiVari

<sup>3</sup>Following [123], we remove the attention mask to avoid inefficiency when a cyclic shift [66] is operated.

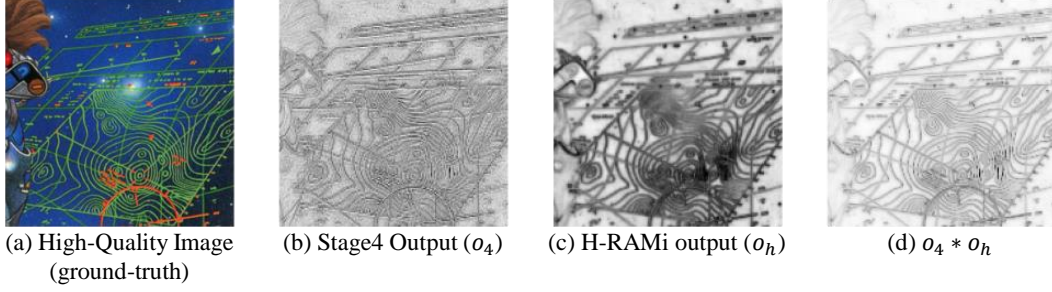


Figure 4: Impacts of H-RAMi. **(a)** A ground-truth high-quality image. **(b)**, **(c)** The feature maps after stage 4 and H-RAMi. **(d)** Element-wise product of **(b)** and **(c)** (Remind Fig. 2a). **(b)**, **(c)**, **(d)** are obtained by max-pooling along channel and standardization. More are in Appendix Sec. A.5.

before layer-norm [4] (a red dashed arrow next to a violet rectangle of Fig. 2b) of the last D-RAMiT blocks in the hierarchical stage 1, 2, 3, 4. After we upsample the resolutions of the mixed bi-dimensional attentions (inputs) into  $H \times W$ , they are concatenated and mixed by our MobiVari. Therefore, our H-RAMi can take advantage of both multi-scale and bi-dimensional attentions, reconsidering where and how much attention to pay semantically and globally. Fig. 4 illustrates the impacts of H-RAMi. The output of stage 4 at **(b)** produces relatively unclear edges for fine-grained areas. This vulnerability stems from less abundant pixel-level information than non-hierarchical networks [56, 123, 5]. However, H-RAMi reconstructs attentive areas and produces clearer borders at **(c)** by taking both pixel- and semantic-level information. As a result, the re-attended feature map at **(d)** contains more apparent boundaries, which enhances the image restoration accuracy (Tab. 5a).

## 4 Experiments

### 4.1 Experimental Setup

**Training.** We randomly cropped low-quality (LQ) images into various sizes of patches according to each task. The training data was augmented by the random horizontal flip and rotation ( $90^\circ$ ,  $180^\circ$ ,  $270^\circ$ ) as done in the recent works [56, 123, 5, 11]. We minimized  $L_1$  pixel-loss between  $I_{RC}$  and a ground truth high-quality image  $I_{HQ}$ :  $\mathcal{L} = \|I_{HQ} - I_{RC}\|_1$  with Adam [48] optimizer. For image super-resolution (SR), 800 high and low resolution image pairs from DIV2K [1] dataset were used. The low-resolution images were acquired by the MATLAB bicubic kernel from corresponding high-resolution images. The color and grayscale image denoising (DN) models were trained on DFBW, a merged dataset of 800 DIV2K, 2,650 Flickr2K [87], 400 BSD500 [3], and 4,744 WED [71] images, following [56, 110, 116, 12]. The random Gaussian noise level  $\sigma$  ranging  $[0, 50]$  was used to get noisy LQ images. For low-light image enhancement (LLE), 1,785 dark and bright image pairs were utilized (485 LOL [102] + 1,300 VE-LOL [63]), which were either captured or synthesized. Next, we trained our deraining (DR) model on 13,711 synthesized rainy and clean image pairs of Rain13K [111] collected from [26, 106, 115, 114, 55]. Other details are in Appendix Sec. B.

**Evaluation.** For SR, we evaluated the performances on the five benchmark datasets, composed of Set5 [6], Set14 [112], BSD100 [73], Urban100 [40], and Manga109 [74]. We calculated PSNR (dB) and SSIM [100] scores on the Y channel of the YCbCr space. The same metrics were calculated for testing DR, which involves Test100 [115] and Rain100H [106] datasets. To test DN performances, Gaussian noise with different levels  $\sigma$  of  $\{15, 25, 50\}$  is added. We reported PSNR and SSIM on the RGB channel of CBSD68 [73], Kodak24 [25], McMaster [121], and Urban100 for color DN and on Y channel of Set12 [118], BSD68 [73], and Urban100 for grayscale DN. The same metrics for color DN were employed to evaluate the LLE performances on 15 LOL [102] and 100 VE-LOL-cap [63] test images. For all tasks, we also recorded the number of parameters for each model.

### 4.2 Qualitative Comparisons

Fig. 5 presents the visual comparisons with other models, which were selected based on existing state-of-the-art studies for each task. The illustration demonstrates that our proposed dimensional and hierarchical attention mixing methods were able to recover more accurate textures and patterns compared to other methods. Our combination of “local and global” and “pixel- and semantic-level” features made our proposed approach effective. More results are provided in Appendix Sec. C.

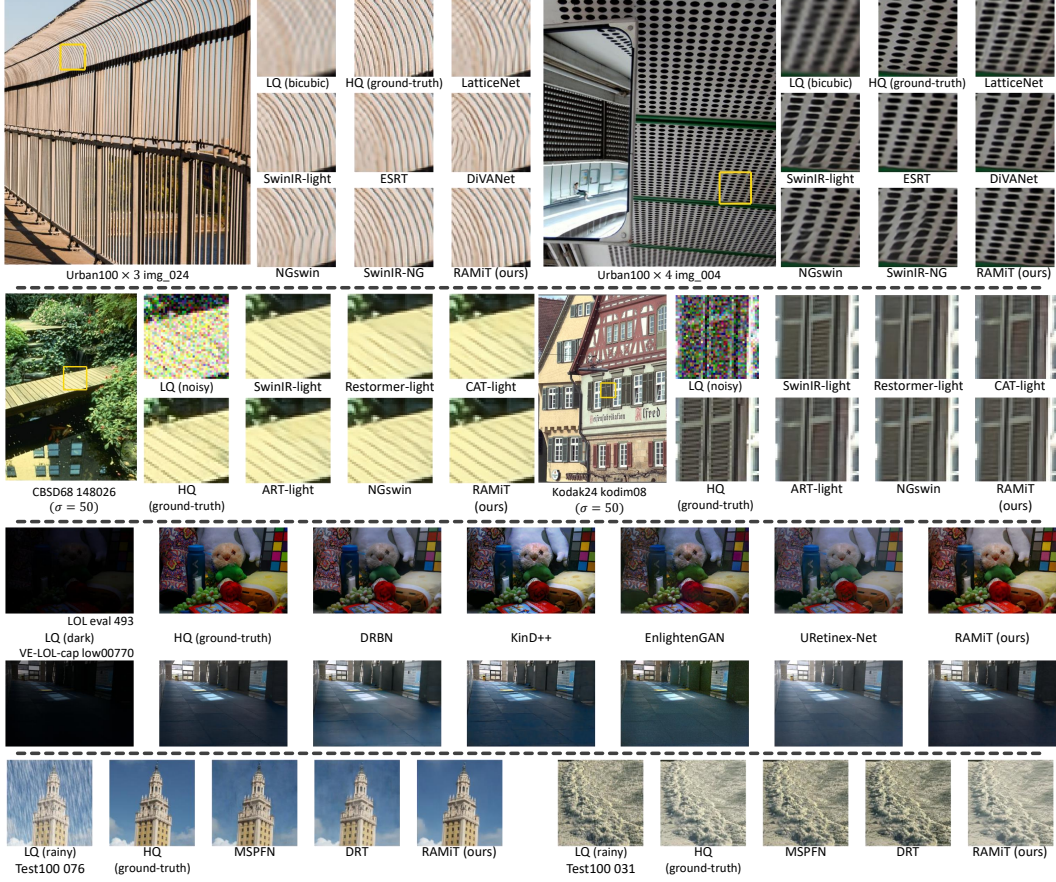


Figure 5: Visual comparisons of multiple lightweight image restoration tasks. LQ: Low-Quality input. HQ: High-Quality target. **(1st row)** Super-Resolution. **(2nd row)** Denoising. **(3rd row)** Low-Light Enhancement. **(4th row)** Deraining. More results are provided in Appendix Sec. C.

### 4.3 Quantitative Comparisons

**Image Super-Resolution (SR).** In Tab. 2, we compared our RAMiT-1 and RAMiT with other state-of-the-art lightweight SR methods, including CARN (ECCV18) [2], LatticeNet (ECCV20) [68], SwinIR-light (ICCVW21) [56], FMEN (CVPRW22) [22], ESRT (CVPRW22) [67], ELAN-light (ECCV22) [123], DiVANet (PR23) [5], NGswin (CVPR23) [11], and SwinIR-NG (CVPR23) [11]. We also reported the number of operations (Mult-Adds) of each model. Our RAMiT-1 outperformed or matched almost all other networks on both PSNR and SSIM with the second-fewest Mult-Adds. In addition, RAMiT gained PSNR up to 0.12dB while consuming only 59.6 ~ 67.7% of the operations used by the latest SwinIR-NG. Especially, RAMiT offers the best trade-off between efficiency and performance on  $\times 2$  and  $\times 4$  tasks among the compared approaches, as it had the third fewest Mult-Adds. For a concern of the number of parameters, see Appendix Sec. A.6.

**Color Image Denoising (CDN).** In Tab. 3a, we referred to the lightweight denoising Transformer baselines introduced by [12], such as SwinIR-light (ICCVW21) [56], Restormer-light (CVPR22) [110], CAT-light (NeurIPS22) [10], ART-light (ICLR23) [116], and NGswin (CVPR23) [11]. Our RAMiT-1 competitively performed on three noise levels with the fewest parameters. It is notable that SwinIR, CAT, and NGswin aimed to boost locality of a window-based spatial self-attention, while Restormer and ART pursued an improved ability in capturing non-local dependency in an image. However, RAMiT surpassed them on every noise level and dataset through both local and global context.

**Grayscale Image Denoising (GDN).** As shown in Tab. 3b, our RAMiT was good at removing noise from the grayscale images as well. RAMiT reconstructed more similar images to ground-truth for human-perception in that our SSIM scores were the highest. Moreover, RAMiT gained PSNR scores on all noise levels up to 0.23dB.



Table 2: Comparison of lightweight **super-resolution** results. RAMiT-1 and RAMiT employ MobileNet V1 and V2 [38, 83] variants (MobiVari<sup>1</sup>), respectively. Mult-Adds is evaluated on a 1280×720 high-resolution image. The best, second best, and third best results are in **red**, **orange**, and **blue**.

Method	Mult-Adds	#Params	Scale	Set5 [6]		Set14 [112]		BSD100 [73]		Urban100 [40]		Manga109 [74]		Average	
				PSNR	SSIM	PSNR	SSIM	PSNR	SSIM	PSNR	SSIM	PSNR	SSIM	PSNR	SSIM
CARN [2]	222.8G	1,592K	×2	37.76	0.9590	33.52	0.9166	32.09	0.8978	31.92	0.9256	38.36	0.9765	34.730	0.93510
LatticeNet [68]	169.5G	756K		38.06	0.9607	33.70	0.9187	32.20	0.8999	32.25	0.9288	38.94	0.9774	35.030	0.93710
SwinIR-light [56]	243.7G	910K		38.14	0.9611	33.86	0.9206	<b>32.31</b>	<b>0.9012</b>	<b>32.76</b>	<b>0.9340</b>	39.12	<b>0.9783</b>	35.238	<b>0.93904</b>
FMEN [22]	172.0G	<b>748K</b>		38.10	0.9609	33.75	0.9192	32.26	0.9007	32.41	0.9311	38.95	0.9778	35.094	0.93794
ESRT [67]	191.4G	<b>677K</b>		38.03	0.9600	33.75	0.9184	32.25	0.9001	32.58	0.9318	39.12	0.9774	35.146	0.93754
ELAN-light [123]	168.4G	<b>582K</b>		<b>38.17</b>	0.9611	<b>33.94</b>	<b>0.9207</b>	<b>32.30</b>	<b>0.9012</b>	<b>32.76</b>	<b>0.9340</b>	39.12	<b>0.9783</b>	35.258	<b>0.93906</b>
DiVANet [5]	189.0G	902K		<b>38.16</b>	<b>0.9612</b>	33.80	0.9195	32.29	<b>0.9012</b>	32.60	0.9325	39.08	0.9775	35.186	0.93838
NGwin [11]	<b>140.4G</b>	998K		38.05	0.9610	33.79	0.9199	32.27	0.9008	32.53	0.9324	38.97	0.9777	35.122	0.93836
SwinIR-NG [11]	274.1G	1,181K		<b>38.17</b>	<b>0.9612</b>	<b>33.94</b>	0.9205	<b>32.31</b>	<b>0.9013</b>	<b>32.78</b>	<b>0.9340</b>	<b>39.20</b>	<b>0.9781</b>	<b>35.280</b>	<b>0.93902</b>
RAMiT-1 (ours)	<b>149.3G</b>	<b>823K</b>	×3	<b>38.18</b>	<b>0.9612</b>	<b>33.89</b>	<b>0.9209</b>	<b>32.30</b>	<b>0.9012</b>	<b>32.71</b>	<b>0.9335</b>	<b>39.22</b>	<b>0.9780</b>	<b>35.260</b>	<b>0.93896</b>
RAMiT (ours)	<b>163.4G</b>	<b>940K</b>		<b>38.16</b>	<b>0.9612</b>	<b>34.00</b>	<b>0.9213</b>	<b>32.33</b>	<b>0.9015</b>	<b>32.81</b>	<b>0.9346</b>	<b>39.32</b>	<b>0.9783</b>	<b>35.324</b>	<b>0.93938</b>
CARN [2]	118.8G	1,592K		34.29	0.9255	30.29	0.8407	29.06	0.8034	28.06	0.8493	33.50	0.9440	31.040	0.82028
LatticeNet [68]	76.3G	<b>765K</b>		34.40	0.9272	30.32	0.8416	29.10	0.8049	28.19	0.8513	33.63	0.9442	31.128	0.82784
SwinIR-light [56]	109.5G	918K		<b>34.62</b>	0.9289	30.54	<b>0.8463</b>	29.20	0.8082	28.66	0.8624	33.98	0.9478	31.400	0.82782
FMEN [22]	77.2G	<b>757K</b>		34.45	0.9275	30.40	0.8435	29.17	0.8063	28.33	0.8562	33.86	0.9462	31.242	0.827594
ESRT [67]	96.4G	770K		34.42	0.9268	30.43	0.8433	29.15	0.8063	28.46	0.8574	33.95	0.9455	31.282	0.827586
ELAN-light [123]	<b>75.7G</b>	<b>590K</b>		34.61	0.9288	<b>30.55</b>	<b>0.8463</b>	29.21	0.8081	<b>28.69</b>	0.8624	34.00	0.9478	31.412	0.827868
DiVANet [5]	89.0G	949K	×4	34.60	0.9285	30.47	0.8447	29.19	0.8073	28.58	0.8603	33.94	0.9468	31.356	0.827752
NGwin [11]	<b>66.6G</b>	1,007K		34.52	0.9282	30.53	0.8456	29.19	0.8078	28.52	0.8603	33.89	0.9470	31.330	0.827778
SwinIR-NG [11]	114.1G	1,190K		<b>34.64</b>	<b>0.9293</b>	<b>30.58</b>	<b>0.8471</b>	<b>29.24</b>	<b>0.8090</b>	<b>28.75</b>	<b>0.8639</b>	<b>34.22</b>	<b>0.9488</b>	<b>31.486</b>	<b>0.827962</b>
RAMiT-1 (ours)	<b>70.7G</b>	<b>832K</b>		<b>34.62</b>	<b>0.9292</b>	<b>30.58</b>	<b>0.8463</b>	<b>29.23</b>	<b>0.8087</b>	<b>28.67</b>	<b>0.8627</b>	<b>34.21</b>	<b>0.9485</b>	<b>31.462</b>	<b>0.827908</b>
RAMiT (ours)	<b>77.3G</b>	<b>949K</b>		<b>34.63</b>	<b>0.9290</b>	<b>30.60</b>	<b>0.8467</b>	<b>29.25</b>	<b>0.8093</b>	<b>28.76</b>	<b>0.8646</b>	<b>34.30</b>	<b>0.9490</b>	<b>31.508</b>	<b>0.827972</b>
CARN [2]	90.9G	1,592K	×4	32.13	0.8937	28.60	0.7806	27.58	0.7349	26.07	0.7837	30.47	0.9084	28.970	0.82026
LatticeNet [68]	43.6G	777K		32.18	0.8943	28.61	0.7812	27.57	0.7355	26.14	0.7844	30.54	0.9075	29.008	0.82058
SwinIR-light [56]	61.7G	930K		<b>32.44</b>	0.8976	<b>28.77</b>	0.7858	27.69	0.7406	26.47	0.7980	30.92	0.9151	29.258	0.82742
FMEN [22]	44.2G	<b>769K</b>		32.24	0.8955	28.70	0.7839	27.63	0.7379	26.28	0.7908	30.70	0.9107	29.110	0.82376
ESRT [67]	67.7G	<b>751K</b>		32.19	0.8947	28.69	0.7833	27.69	0.7379	26.39	0.7962	30.75	0.9100	29.142	0.82442
ELAN-light [123]	43.2G	<b>601K</b>		32.43	0.8975	<b>28.78</b>	0.7858	27.69	0.7406	<b>26.54</b>	0.7982	30.92	0.9150	29.272	0.82742
DiVANet [5]	57.0G	939K		32.41	0.8973	28.70	0.7844	27.65	0.7391	26.42	0.7958	30.73	0.9119	29.182	0.82570
NGwin [11]	<b>36.4G</b>	1,019K		32.33	0.8963	<b>28.78</b>	<b>0.7859</b>	27.66	0.7396	26.45	0.7963	30.80	0.9128	29.204	0.82618
SwinIR-NG [11]	63.0G	1,201K		<b>32.44</b>	<b>0.8980</b>	<b>28.83</b>	<b>0.7870</b>	<b>27.73</b>	<b>0.7418</b>	<b>26.61</b>	<b>0.8010</b>	<b>31.09</b>	<b>0.9161</b>	<b>29.340</b>	<b>0.82878</b>
RAMiT-1 (ours)	<b>38.6G</b>	<b>844K</b>	×4	<b>32.54</b>	<b>0.8987</b>	<b>28.73</b>	<b>0.7856</b>	<b>27.70</b>	<b>0.7408</b>	<b>26.51</b>	<b>0.7996</b>	<b>31.05</b>	<b>0.9156</b>	<b>29.306</b>	<b>0.82806</b>
RAMiT (ours)	<b>42.1G</b>	<b>961K</b>		<b>32.56</b>	<b>0.8992</b>	<b>28.83</b>	<b>0.7873</b>	<b>27.71</b>	<b>0.7418</b>	<b>26.60</b>	<b>0.8017</b>	<b>31.17</b>	<b>0.9170</b>	<b>29.374</b>	<b>0.82940</b>

Table 3: Comparison of lightweight **blind image denoising** results. We refer to the baselines in [12].

(a) Color Image Denoising (CDN).

(b) Grayscale Image Denoising (GDN).

Method	#Params	$\sigma$	CSD68 [1]		Kodak24 [1]		McMaster [1]		Urban100 [1]		Method	#Params	$\sigma$	Set12 [113]		BSD68 [1]		Urban100 [1]	
			PSNR	SSIM	PSNR	SSIM	PSNR	SSIM	PSNR	SSIM				PSNR	SSIM	PSNR	SSIM	PSNR	SSIM
SwinIR-light [56]	<b>905K</b>	15	<b>34.16</b>	<b>0.9323</b>	<b>35.18</b>	<b>0.9359</b>	<b>35.23</b>	<b>0.9295</b>	<b>34.50</b>	<b>0.9478</b>	SwinIR-light [56]	<b>903K</b>	15	<b>33.04</b>	<b>0.9052</b>	<b>31.78</b>	<b>0.8926</b>	<b>33.04</b>	<b>0.9317</b>
Restormer-light [110]	1,054K		33.99	0.9311	34.86	0.9244	34.69	0.9229	34.00	0.9439	Restormer-light [110]	1,053K		32.93	0.9039	31.76	0.8922	32.81	0.9306
CAT-light [110]	1,042K		34.01	0.9304	34.90	0.9237	34.83	0.9247	34.12	0.9443	CAT-light [110]	1,041K		32.91	0.9021	31.89	0.8913	31.80	0.9306
ART-light [116]	1,084K		34.08	0.9315	35.00	0.9251	35.10	0.9282	34.44	0.9467	ART-light [116]	1,082K		32.93	0.9023	31.73	0.8911	32.89	0.9299
NGwin [11]	993K		<b>34.12</b>	<b>0.9324</b>	<b>35.12</b>	<b>0.9268</b>	<b>35.17</b>	<b>0.9294</b>	<b>34.53</b>	<b>0.9476</b>	NGwin [11]	<b>991K</b>		<b>33.04</b>	<b>0.9055</b>	<b>31.78</b>	<b>0.8927</b>	<b>32.99</b>	<b>0.9344</b>
RAMiT-1 (ours)	<b>818K</b>		<b>34.16</b>	<b>0.9324</b>	<b>35.13</b>	<b>0.9264</b>	<b>35.22</b>	<b>0.9297</b>	<b>34.58</b>	<b>0.9478</b>	RAMiT (ours)	<b>932K</b>		<b>33.14</b>	<b>0.9070</b>	<b>31.82</b>	<b>0.8939</b>	<b>33.19</b>	<b>0.9346</b>
RAMiT (ours)	<b>935K</b>	25	<b>34.23</b>	<b>0.9332</b>	<b>35.22</b>	<b>0.9276</b>	<b>35.31</b>	<b>0.9309</b>	<b>34.68</b>	<b>0.9488</b>	SwinIR-light [56]	<b>903K</b>	25	<b>30.67</b>	<b>0.8669</b>	29.32	<b>0.8325</b>	<b>30.32</b>	<b>0.8963</b>
SwinIR-light [56]	<b>905K</b>		<b>31.50</b>	<b>0.8883</b>	<b>32.69</b>	<b>0.8868</b>	<b>32.90</b>	<b>0.8977</b>	<b>33.23</b>	<b>0.9222</b>	Restormer-light [110]	1,053K		30.60	0.8659	29.32	0.8322	30.32	0.8952
Restormer-light [110]	1,054K		31.33	0.8865	32.38	0.8833	32.44	0.8905	31.60	0.9161	CAT-light [110]	1,041K		30.60	0.8641	29.47	0.8330	29.32	0.8393
CAT-light [110]	1,042K		31.37	0.8855	32.43	0.8822	32.58	0.8928	31.75	0.9167	ART-light [116]	1,082K		30.52	0.8620	29.25	0.8285	30.30	0.8919
ART-light [116]	1,084K		31.40	0.8864	32.49	0.8833	32.74	0.8956	32.03	0.9195	NGwin [11]	<b>991K</b>		<b>30.65</b>	<b>0.8671</b>	29.33	0.8324	<b>30.46</b>	<b>0.8961</b>
NGwin [11]	993K		<b>31.44</b>	<b>0.8884</b>	<b>32.61</b>	<b>0.8865</b>	<b>32.82</b>	<b>0.8978</b>	<b>32.13</b>	<b>0.9215</b>	RAMiT (ours)	<b>932K</b>		<b>30.79</b>	<b>0.8694</b>	<b>29.37</b>	<b>0.8346</b>	<b>30.71</b>	<b>0.9013</b>
RAMiT-1 (ours)	<b>818K</b>	50	<b>31.50</b>	<b>0.8888</b>	<b>32.64</b>	<b>0.8862</b>	<b>32.91</b>	<b>0.8989</b>	<b>32.21</b>	<b>0.9223</b>	SwinIR-light [56]	<b>903K</b>	50	<b>27.50</b>	<b>0.7966</b>	26.35	<b>0.7299</b>	<b>27.01</b>	<b>0.8190</b>
RAMiT (ours)	<b>935K</b>		<b>31.59</b>	<b>0.8902</b>	<b>32.76</b>	<b>0.8887</b>	<b>33.02</b>	<b>0.9008</b>	<b>32.36</b>	<b>0.9244</b>	Restormer-light [110]	1,053K		27.48	0.7960	26.38	0.7285	26.92	0.8190
SwinIR-light [56]	<b>905K</b>		<b>28.22</b>	<b>0.8006</b>	<b>29.54</b>	<b>0.8039</b>	<b>29.71</b>	<b>0.8339</b>	<b>28.89</b>	<b>0.8658</b>	CAT-light [110]	1,041K		27.49	0.7935	<b>26.52</b>	<b>0.7333</b>	26.06	0.7456
Restormer-light [110]	1,054K		28.04	0.7974	29.19	0.8034	29.31	0.8256	28.30	0.8559	ART-light [116]	1,082K		<b>27.26</b>	<b>0.7856</b>	26.25	0.7194	26.68	0.8065
CAT-light [110]	1,042K		28.11	0.7960	29.29	0.8024	29.48	0.8296	28.46	0.8573	NGwin [11]	<b>991K</b>		<b>27.38</b>	<b>0.7960</b>	<b>26.35</b>	<b>0.7299</b>	<b>26.92</b>	<b>0.8190</b>
ART-light [116]	1,084K		28.08	0.7950	29.27	0.8000	29.48	0.8279	28.62	0.8584	RAMiT (ours)	<b>932K</b>		<b>27.65</b>	<b>0.8013</b>	<b>26.46</b>	<b>0.7333</b>	<b>27.32</b>	<b>0.8306</b>
NGwin [11]	993K	<b>28.13</b>	<b>0.8011</b>	<b>29.42</b>	<b>0.8087</b>	<b>29.59</b>	<b>0.8339</b>	<b>28.75</b>	<b>0.8644</b>										
RAMiT-1 (ours)	<b>818K</b>	50	<b>28.24</b>	<b>0.8024</b>	<b>29.51</b>	<b>0.8083</b>	<b>29.74</b>	<b>0.8376</b>	<b>28.93</b>	<b>0.8671</b>									
RAMiT (ours)	<b>935K</b>		<b>28.37</b>	<b>0.8058</b>	<b>29.67</b>	<b>0.8143</b>	<b>29.91</b>	<b>0.8422</b>	<b>29.15</b>	<b>0.8729</b>									



Table 4: Comparison of lightweight **low-light image enhancement** and **image deraining** results.

(a) Low-Light Image Enhancement (LLE).						(b) Image Deraining (DR).					
Method	#Params	LOL [102]		VE-LOL-cap [63]		Method	#Params	Test100 [115]		Rain100H [106]	
		PSNR	SSIM	PSNR	SSIM			PSNR	SSIM	PSNR	SSIM
DRBN [107]	558K	18.80	0.8304	20.11	0.8545	UMRL [108]	984K	24.41	0.8290	26.01	0.8320
KinD++ [124]	8,275K	21.80	0.8338	22.21	0.8430	MSPFN [44]	13,350K	27.50	0.8760	28.66	0.8600
EnlightenGAN [46]	8,640K	17.48	0.6507	18.64	0.6754	DRT [57]	1,180K	27.02	0.8470	29.47	0.8460
URetinet-Net [104]	361K	21.33	0.8348	21.22	0.8593	TAO-Net [54]	755K	28.59	0.8870	28.96	0.8640
<b>RAMiT (ours)</b>	<b>935K</b>	<b>24.14</b>	<b>0.8423</b>	<b>28.73</b>	<b>0.8886</b>	<b>RAMiT (ours)</b>	<b>935K</b>	<b>30.44</b>	<b>0.9012</b>	<b>29.69</b>	<b>0.8775</b>

Table 5: Ablation studies on our proposed methods. The reported PSNR scores represent the average values on the benchmark test datasets of each image restoration task provided in Tabs. 2, 3, 4. Mult-Adds is calculated on a  $1280 \times 720$  high-quality image.

(a) D-RAMiT & H-RAMi (Mult-Adds / #Params / Average PSNR).											
Transformer	H-RAMi	SR $\times 2$		SR $\times 4$		CDN $\sigma = 50$		LLE		DR	
Pure CHSA	w/	153.4G / 957K / 34.994	39.6G / 978K / 29.074	583.2G / 952K / 28.848	583.2G / 952K / 23.985	583.2G / 952K / 28.810		583.2G / 952K / 23.985	583.2G / 952K / 28.810		{i}
Pure SPSSA	w/o	168.6G / 955K / 35.218	43.4G / 976K / 29.302	641.2G / 950K / 29.010	641.2G / 950K / 25.095	641.2G / 950K / 29.175		641.2G / 950K / 25.095	641.2G / 950K / 29.175		{ii}
Pure SPSSA	w/	173.4G / 975K / 35.276	44.6G / 996K / 29.342	659.9G / 970K / 29.128	659.9G / 970K / 25.140	659.9G / 970K / 29.190		659.9G / 970K / 25.140	659.9G / 970K / 29.190		{iii}
D-RAMiT	w/o	158.5G / 920K / 35.310	40.9G / 940K / 29.338	602.1G / 914K / 29.205	602.9G / 914K / 26.365	602.1G / 914K / 29.940		602.9G / 914K / 26.365	602.1G / 914K / 29.940		{iv}
D-RAMiT	w/	163.4G / 940K / <b>35.324</b>	42.1G / 961K / <b>29.374</b>	620.8G / 935K / <b>29.275</b>	621.6G / 935K / <b>26.435</b>	620.8G / 935K / <b>30.065</b>		621.6G / 935K / <b>26.435</b>	620.8G / 935K / <b>30.065</b>		{v}

(b) Reciprocal Helper (w/o / w/).				(c) MobiVari Activation Function.			
Task	Mult-Adds (G)		PSNR	Activation	SR $\times 2$	CDN $\sigma = 50$	LLE
SR $\times 2$	163.2 / 163.4		35.308 / <b>35.324</b>	ReLU6 [38, 83]	35.304	29.220	25.530
SR $\times 3$	77.16 / 77.26		31.482 / <b>31.508</b>	ReLU [78]	35.322	29.270	26.160
SR $\times 4$	42.08 / 42.13		29.308 / <b>29.374</b>	GELU [34]	35.320	29.268	26.230
LLE	620.8 / 621.6		25.915 / <b>26.435</b>	Swish <sub><math>\beta=1</math></sub> [81]	35.306	29.250	26.160
				LeakyReLU [72]	<b>35.324</b>	<b>29.275</b>	<b>26.435</b>

CHSA and the narrow receptive field of SPSSA. Our method achieved better results on multiple tasks with fewer computations and parameters than SPSSA. This effectiveness is also observed without the H-RAMi layer, another proposed method ({ii} vs. {iv}). Moreover, as shown in Tab. 5b, the reciprocal helper contributed to the improvement. Note that this approach consumed only minor amounts of Mult-Adds and no extra parameters. Therefore, it was proven that our dimensional reciprocal self-attention mixing Transformers could be suitable for general IR tasks.

**H-RAMi.** Tab. 5a ({ii} vs. {iii}, {iv} vs. {v}) revealed that H-RAMi constituted another critical component, not only for our D-RAMiT but also for a pure SPSSA. Regardless of tasks, this layer enabled the models to remain robust even when a hierarchical network caused information losses. We assumed that since a noisy image contained more distorted boundaries, the impacts of H-RAMi that could recover more accurate object boundaries (Sec. 3.3) were particularly significant in denoising tasks. Additionally, the results highlighted the remarkable efficiency in that H-RAMi required marginal additional operations and parameters, which accounted for a maximum of only 3.01% and 2.25% of the total costs, respectively.

**MobiVari.** In Tab. 5c, we investigated different non-linear activation functions for our MobiVari. LeakyReLU [72] resulted in the best stable performances across multiple tasks and was selected as the default option. Such stability of LeakyReLU can be attributed to its ability to better preserve relatively large absolute negative values compared to other activation functions. These values, which are occasionally generated by intermediate layers, may have a subtle influence on a feature map, ultimately leading to a significant difference in the final output of a network.

## 5 Conclusion

This paper proposed the Reciprocal Attention Mixing Transformers (RAMiT). To incorporate local and global context in an image, our Dimensional Reciprocal Attention Mixing Transformer (D-RAMiT) blocks computed bi-dimensional self-attentions in parallel and mixed them. The reciprocal helper was useful for this mechanism. Moreover, the Hierarchical Reciprocal Attention Mixing (H-RAMi) layer was also introduced, where the information losses caused by the downsampled features were complemented. For mixing attentions and other convolutional layers, we revisited and modified the popular MobileNets. As a result, our RAMiT achieved state-of-the-art performances on multiple lightweight image restoration tasks, including super-resolution, color denoising, grayscale denoising, low-light enhancement, and deraining. In closing, we hope this work can be further developed and extended to other low-level tasks as well as high-level vision.

## Acknowledgments and Disclosure of Funding

This paper was supported by Institute of Information & Communications Technology Planning & Evaluation (IITP) grant (No.2022-0-00956) and Korea Health Industry Development Institute (KHIDI) grant (No. H122C1983) funded by the Korea government (MSIT). Special thanks to Prof. Dr. Dasaem Jeong for valuable advises.

## APPENDIX

### A Supplementary Discussions and Ablation Studies

In this section, we provide a detailed description of our methods with comprehensive and intuitive illustrations that were omitted from the main content due to page limit. We also discuss our novelty and superiority over existing networks or limitation. Additionally, we provide some additional ablation studies for comprehensive understanding of the proposed RAMiT.

#### A.1 MobiVari (MobileNet Variants) and Reconstruction Module

We revisit MobileNet V1 & V2 architectures [38, 83] to incorporate simple and efficient CNN structures into our components. Fig. A illustrates a comparison between the MobileNets and our modified versions. We replace the ReLU6 non-linearity [83] with LeakyReLU [72] to preserve subtle gradients that ReLU6 cannot capture [72]. Empirical evidence in Tab. 5c of the main paper shows that this change is the most stable. The  $3 \times 3$  depth-wise ( $dw$ ) and  $1 \times 1$  point-wise ( $pw$ ) convolutions in MobileNets are residually connected [33] with the input feature. However, if the channels produced by  $pw$  convolutions differ from input channels, the skip connection for  $pw$  convolutions is ignored. Furthermore, because the first  $1 \times 1$  convolution expanding channels in MobileNet V2 requires many parameters and computations, it is not suitable for our lightweight design. Therefore, we substitute it with group convolution [13], where the group size and expansion ratio are set to 4 and 1.2, respectively, by default. When a network selects MobiVari 1, we denote it as RAMiT-1 (RAMiT uses MobiVari 2). Our MobiVari is applied to attention mixing layers of D-RAMiT and H-RAMiT, a downsizing layer, a bottleneck, and the reconstruction module.

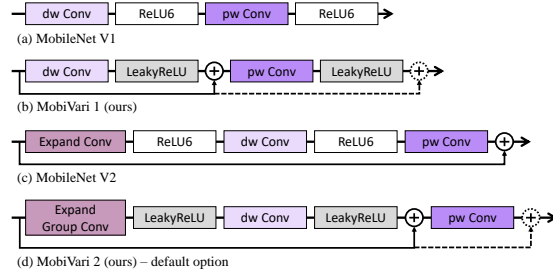


Figure A: Comparison of MobileNets V1 & V2 and our corresponding variants, MobiVari 1 & 2.

Fig. B depicts the reconstruction module (a final layer). The basic structure follows the reconstruction module of NGswin [11]. The only difference is that we place two MobiVari layers before the default version to balance the trade-off between performance and efficiency (See Fig. C). This module slightly varies depending on tasks. For super-resolution, a pixel-shuffler [85] is employed to upscale the feature maps by  $r$  times. However, since other tasks (denoising, low-light enhancement, and deraining) do not require this process, the pixel-shuffler is discarded. The symbols and numbers in parentheses indicate changes of channels. The operation  $I_{res} + I_{LQ}$  follows convention [56, 110].

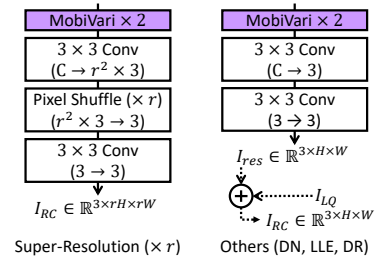


Figure B: Reconstruction module.

#### A.2 Bi-dimensional Self-Attention

Similar to our bi-dimensional self-attention of the proposed D-RAMiT blocks, DaViT [16] also developed a Transformer using both spatial self-attention (SPSA) and channel self-attention (CHSA). Tab. Aa summarizes the attributes of DaViT and D-RAMiT. A core difference is that DaViT “alternatively” places SPSA and CHSA, while D-RAMiT operates them “in parallel”. As discussed in Sec. 3.2 of the main text, our architecture can boost (depending on tasks) both SPSA and CHSA

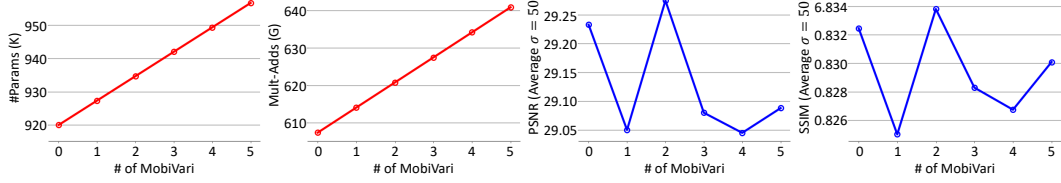


Figure C: Ablation study on the number of MobiVari layers at the reconstruction module. The metrics are evaluated on color denoising task using  $\sigma = 50$ . PSNR and SSIM average the scores on four benchmark datasets.

through the reciprocal helper, which DaViT fundamentally cannot utilize. Another crucial distinction is related to “which self-attention module is given more importance”. While D-RAMiT assigns more multi-heads on SPSA, DaViT makes the number of both modules identical. We hypothesize that DaViT’s simple approach is unsuitable for lightweight image restoration because although CHSA can capture global dependency, its performance is significantly impaired under parameter constraints, as observed in Tab. 5a of our main body. Therefore, more weights on SPSA can be more useful for constructing an effective lightweight RAMiT. Other differences are summarized in the table.

To further demonstrate our superiority over the simple bi-dimensional approach of DaViT, we constructed two versions in Tab. Ab. The first version, DaViT-*full*, replaced the D-RAMiT blocks’ elements in Tab. Aa with those of DaViT. The second version, DaViT-*core*, changed only the core designs (*i.e.*, SPSA & CHSA “Operating” and “Importance on”) from ours to those of DaViT, while the parts of the “Existing Elements Employed” column remained as our settings. The other elements not mentioned in the table followed our default settings for a fair comparison, including the shallow module, MobiVari, the downsizing layers, the bottleneck layer, H-RAMi layer, the reconstruction module, and the hyper-parameters of Tab. F (except that `chsa_head_ratio` is no longer needed). The results show that RAMiT outperformed both DaViT versions while having fewer parameters and almost the same Mult-Adds. It is demonstrated that our meticulous composition of SPSA and CHSA can make a significant difference for multiple lightweight image restoration tasks.

Table A: Comparisons of RAMiT and DaViT [16].

(a) Attribute comparisons. The text in **bold** indicates the key differences. “LN” represents whether the position of layer-norm [4] is before (Pre) or after (Post) the self-attention and feed-forward network.

Method	SPSA & CHSA		Existing Elements Employed				Solving Problems
	Operating	Importance on	Window Shift	Positional Encoding	Self-Attention	LN	
DaViT [16]	Alternatively	Both equally	No use	Convolution [43]	Scaled dot-product [92]	Pre [21]	High-level vision
D-RAMiT (ours)	In parallel	SPSA more	Cyclic [66]	Relative Position Bias [34, 66]	Scaled cosine [65]	Post [65]	Low-level vision

(b) Ablation study on DaViT (Mult-Adds / #Params / Average PSNR).

Method	SR $\times 2$	SR $\times 4$	CDN $\sigma = 50$	LLE	DR
DaViT- <i>full</i> [16]	167.0G / 983K / 35.064	43.0G / 1,003K / 29.088	635.2G / 977K / 28.785	635.2G / 977K / 20.965	635.2G / 977K / 27.910
DaViT- <i>core</i> [16]	163.2G / 966K / 35.172	42.08G / 987K / 29.268	620.8G / 961K / 29.108	620.8G / 961K / 26.000	620.8G / 961K / 29.630
RAMiT (ours)	<b>163.4G / 940K / 35.324</b>	<b>42.13G / 961K / 29.374</b>	<b>620.8G / 935K / 29.275</b>	<b>621.6G / 935K / 26.435</b>	<b>620.8G / 935K / 30.065</b>

### A.3 LAM Comparisons with Other Models

SwinIR-light (ICCVW21) [56] is the first successful attempt applying window self-attention (WSA) to the image restoration tasks. Most recently, SwinIR-NG (CVPR23) [11] defined an N-Gram context method enlarging the regions viewed for recovering distorted pixels, to solve the limited “local” receptive field problem of SwinIR-light. However, SwinIR-NG failed to capture “global context”, while our RAMiT successfully exploit the “global receptive field” maintaining WSA approach, which is clarified by LAM [28] results in Fig. D. Even if SwinIR-NG tends to utilize the slightly expanded receptive field when compared to SwinIR-light, the gradients of SwinIR-NG that actually contribute to reconstruct a small red box are limited within “local areas”. By contrast, our RAMiT can convey the gradients to “global regions”, which improves low-level vision performances with fewer computational costs than SwinIR-NG (reference Tab. 2 of the main paper).

This ability results from adoption of channel self-attention. According to prior work, Squeeze-and-Excitation networks [39], the channel-attention can effectively embed the “global feature responses”. RCAN [125] delivered an insight that channel-wise attention would be good at modeling “global spatial dependency” for low-level vision tasks. Afterwards, Restormer [110] applied this mechanism

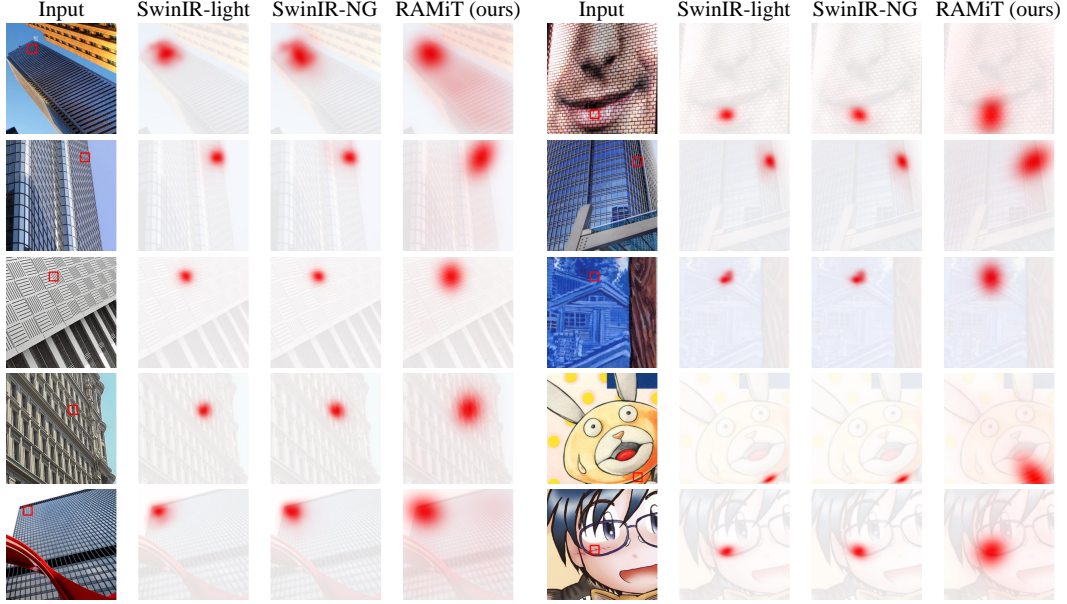


Figure D: Local Attribution Map (LAM) [28] comparison. The depth of the red areas indicates the extent to which the regions contribute to recovering a red box of an input.

to self-attention without squeeze operations, thereby preserving abundant spatial information, which enabled the image restoration networks to more effectively capture the “global interdependencies” in a whole image. Exploiting such advantages of channel self-attention and the effective WSA, RAMiT can yield meaningfully larger receptive fields than the “pure local-attention” of the SwinIR family. Therefore, our work can be considered an enhanced version of the N-Gram context [11], which extends the “local” N-Gram approach to a “Global-Gram” method.

#### A.4 Reciprocal Helper

As proved in Tab. 5b of the main content, our Reciprocal Helper<sup>4</sup> can boost  $\times 2, \times 3, \times 4$  super-resolution and low-light enhancement tasks. However, Tab. B shows that this mechanism is unable to improve the performances of denoising and deraining. We interpret this limitation in terms of properties of the tasks. Degradation used for the super-resolution and low-light enhancement inputs relatively has regularity and therefore may be easy to be globally encoded. This property may make our reciprocal helper useful for the parallel process of local and global self-attention. On the other hand, when dealing with denoising or deraining low-quality inputs, the network is required to erase somethings that obscure the high-quality objects or background. Since it is ill-posed to globally encode these (randomly) disorganized obstructions with a small network capacity, the global embeddings produced by the channel attention may confuse the spatial attention module of the next blocks. However, if the parallel process lacks the reciprocal helper, the MobiVari mixing layers alone can still resolve this issue well. Admitting this limitation, we will conduct more sophisticated future work on other helper algorithms that can improve universal tasks. Nevertheless, our core ideas, *i.e.*, dimensional and hierarchical reciprocal self-attention methods, have been already demonstrated to be effective and efficient enough to achieve new state-of-the-art denoising and deraining.

Table B: Ablation study on the proposed Reciprocal Helper for denoising and deraining (w/o / w/).

Task	Mult-Adds (G)	PSNR
Color Denoising	620.8 / 621.6	<b>29.275</b> / 29.253
Grayscale Denoising	618.5 / 619.3	<b>27.143</b> / 27.100
Deraining	620.8 / 621.6	<b>30.065</b> / 29.960

<sup>4</sup>To prevent any confusion, we adopted the term “*Dimensional Reciprocal Attention Mixing Transformer*” (D-RAMiT) to indicate that *every dimension* (spatial and channel) of feature maps is utilized in calculating *self-attention*, and the outcomes are subsequently *mixed* by MobiVari. Consequently, this implies that the reciprocal helper is not a prerequisite to represent dimensional reciprocal attention.



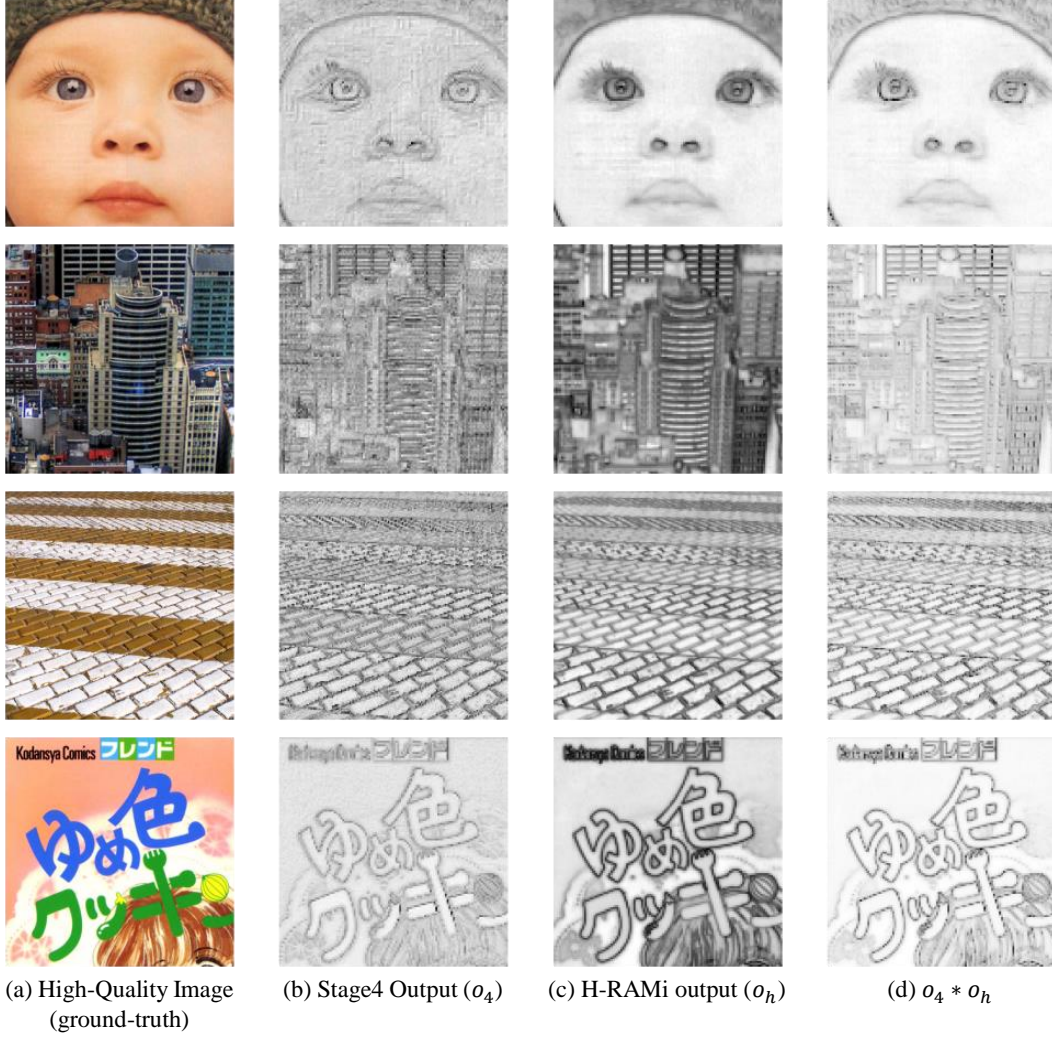


Figure E: Impacts of H-RAMi. (a) A ground-truth high-quality image. (b), (c) The feature maps after stage 4 and H-RAMi. (d) Element-wise product of (b) and (c). (b), (c), (d) are obtained by max-pooling along channel and standardization.

#### A.5 Hierarchical Reciprocal Attention Mixing Layer (H-RAMi)

Although H-RAMi may appear similar to the attention banks used in DiVANet [5], there are notable differences. DiVANet uses non-hierarchical attentions for every residual convolution block, increasing computational costs (see Tab. Ca) and failing to learn semantic-level representation. Moreover, the vertical and horizontal squeeze operations prevent the attention layers from considering full-resolution information. In contrast, our approach reduces time complexity and utilizes semantic-level information by processing compressed feature maps. Furthermore, the inputs to H-RAMi are intermediate attentions from D-RAMiT blocks, which preserve information from both full-resolution spatial and channel self-attentions. We provide additional visual evidences of the benefits in Fig. E. As previously stated in Fig. 4 of the main text, the stage 4 output alone at (b) produces relatively unclear or incorrect edges, which are resolved at (d) by the clearer edges produced by H-RAMi at (c).

#### A.6 Super-Resolution (SR)

Fig. F illustrate trade-offs between efficiency (Mult-Adds, #Params) and performance (average PSNR) on SR tasks, including our RAMiT-slimSR (Tab. Ca), RAMiT-1, and RAMiT. Our methods deliver the best trade-off among the comparative models.

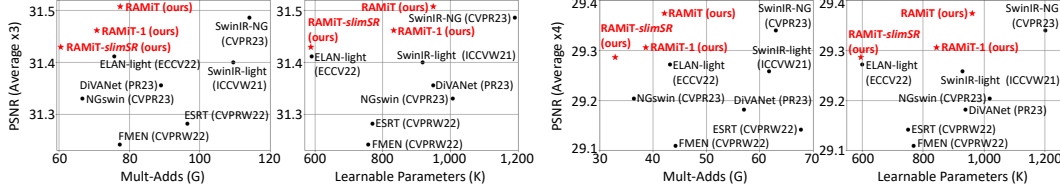


Figure F: Trade-off between efficiency and performance on super-resolution. (Left)  $\times 2$ . (Right)  $\times 4$ .

Tab. 2 of the main text appears to have an unfair aspect. Some networks have fewer parameters than our RAMiT, such as FMEN (CVPRW22) [22], ESRT (CVPRW22) [67], ELAN-light (ECCV22) [123], and DiVANet (PR23) [5]. Although they require more Mult-Adds than RAMiT, it can be questioned whether our improvement is attributed to the proposed design or the result of having simply more parameters. We address this issue in Tab. Ca. The channel (network dimension) and depths (D-RAMiT blocks in stage 1 to 4) of RAMiT were scaled from 64 and [6, 4, 4, 6] to 48 and [8, 2, 2, 8], respectively. In the bottleneck and H-RAMi, we also changed the group size and expansion ratio of MobiVari from 4 and 1.2 to 1 and 2.0, respectively. The group size and expansion ratio of the other MobiVari layers were retained as the default settings. Consequently, we got a compact network denoted as RAMiT-slimSR, which is composed of the fewest learnable parameters and Mult-Adds among the comparative methods. Note that RAMiT-slimSR consumes fewer computations than NGswin (CVPR23) [11], which required the fewest Mult-Adds in Tab. 2. RAMiT-slimSR still outperformed others, showing that our advancements on super-resolution were attributed to the effectiveness and efficiency of the novel approaches.

Furthermore, as shown in Tab. Cb, we found room for improvement of RAMiT with more training data. In addition to 800 images of DIV2K [1] used by RAMiT for super-resolution in Tab. 2 of the main text, many recent studies utilized 2,650 Flickr2K [87] dataset as well to reinforce their SR networks [56, 128, 22, 10, 123]. Following them, we additionally trained our models on DF2K (DIV2K + Flickr2K) for the enhanced performances. The impacts on all upscaling tasks were observed.

Table C: Ablation study on model size and training dataset for super-resolution.

(a) Comparison for RAMiT-slimSR. The best, second best, and third best results are in red, orange, and blue. PSNR and SSIM scores average the results on the five benchmark test datasets.

	Scale	Method						
		FMEN [22]	ESRT [67]	ELAN-light [123]	DiVANet [5]	NGswin [11]	RAMiT-slimSR	RAMiT
Mult-Adds / #Params PSNR / SSIM	×2	172.0G / 748K 35.094 / 0.93794	191.4G / 677K 35.146 / 0.93754	168.4G / 582K 35.258 / 0.93906	189.0G / 902K 35.186 / 0.93838	140.4G / 998K 35.122 / 0.93836	127.8G / 581K 35.226 / 0.93880	163.4G / 940K 35.324 / 0.93938
		PSNR / #Params PSNR / SSIM	×3	77.2G / 757K 31.242 / 0.87594	96.4G / 770K 31.282 / 0.87586	75.7G / 590K 31.412 / 0.87868	89.0G / 949K 31.356 / 0.87752	66.6G / 1.007K 31.330 / 0.87778
Mult-Adds / #Params PSNR / SSIM	×4			44.2G / 769K 29.110 / 0.82376	67.7G / 751K 29.142 / 0.82442	43.2G / 601K 29.272 / 0.82742	57.0G / 939K 29.182 / 0.82570	36.4G / 1.019K 29.204 / 0.82618

(b) Training dataset size of RAMiT.

Dataset (#Images)	Scale	Set5 [6]		Set14 [112]		BSD100 [73]		Urban100 [40]		Manga109 [74]		Average	
		PSNR	SSIM	PSNR	SSIM	PSNR	SSIM	PSNR	SSIM	PSNR	SSIM	PSNR	SSIM
DIV2K (800)	$\times 2$	38.16	0.9612	34.00	0.9213	32.33	0.9015	32.81	0.9346	39.32	0.9783	35.324	0.93938
		38.19	0.9613	33.95	0.9215	32.35	0.9017	32.90	0.9352	39.44	0.9788	35.366	0.93970
DF2K (3,450)	$\times 3$	34.63	0.9290	30.60	0.8467	29.25	0.8093	28.76	0.8646	34.30	0.9490	31.508	0.87972
		34.69	0.9295	30.60	0.8468	29.28	0.8097	28.80	0.8656	34.40	0.9494	31.554	0.88020
DIV2K (800)	$\times 4$	32.56	0.8992	28.83	0.7873	27.71	0.7418	26.60	0.8017	31.17	0.9170	29.374	0.82940
		32.58	0.8995	28.87	0.7876	27.73	0.7419	26.65	0.8036	31.25	0.9174	29.416	0.83000
DF2K (3,450)	$\times 4$												

## A.7 Low-Light Enhancement (LLE)

Tab. D compares MAXIM (CVPR22) [90] and RAMiT to present the effectiveness and efficiency of our model for the LLE task. MAXIM has shown outstanding results on the general image restoration tasks with a large model size. Surprisingly, our RAMiT outperformed MAXIM in terms of average PSNR scores on the 15 images LOL evaluation dataset [102]. Notably, we achieved this impressive result using only 6.63% parameters of MAXIM. Additionally, RAMiT showed lower variance for the evaluated images than MAXIM, indicating more stable restoration of dark images into brighter ones. The visual results are in Fig. G.

Table D: Comparison of MAXIM [90] and RAMiT on low-light enhancement. The PSNR (dB) scores on 15 LOL [102] evaluation images are reported. The numbers in the first row indicate the testing file (.png) names. Std.: standard-deviation.

Model	#Params	001	022	023	055	079	111	146	179	493	547	665	669	748	778	780	Mean	Std.
MAXIM [90]	14,100K	20.98	28.68	24.89	18.83	27.16	17.82	23.30	19.65	13.79	15.66	28.34	28.63	29.96	25.02	28.51	23.41	5.11
RAMiT (ours)	935K	20.50	26.20	19.34	18.74	28.18	31.12	25.74	23.61	20.39	18.32	26.67	25.17	28.07	21.76	28.32	24.14	3.93



Figure G: Visual comparisons of MAXIM [90] and RAMiT. Despite even fewer parameters, RAMiT can restore the extremely dark images with better or matched accuracy compared to MAXIM. In the bottom row, the cases in which RAMiT is highly defeated by MAXIM are provided as well.

Secondarily, we reported a fair comparison with URetinex-Net (CVPR22) [46] in Tab. Ea. This method requires only 38.6% parameters of RAMiT, which can provoke a concern of unfairness. To handle this issue, the channel (network dimension) and the depths (D-RAMiT blocks in stage 1 to 4) of RAMiT were reduced from 64 to 48 and from [6, 4, 4, 6] to [4, 2, 2, 4], respectively. In the bottleneck and H-RAMi, the group size of MobiVari is changed from 4 to 3. As a result, we obtained a downsized model composed of fewer parameters than URetinex-Net, and called it RAMiT-*slimLLE*. RAMiT-*slimLLE* still outperformed URetinex-Net by PSNR margins of up to 7.16dB, which emphasizes our effectiveness and efficiency.

## A.8 Deraining (DR)

Tab. Eb shows our efficiency for deraining task. MPRNet (CVPR21) [111] made advancements on multiple image restoration tasks a few years ago. However, RAMiT can outperform it with 25.7% parameters of MPRNet on a deraining benchmark dataset, such as Test100 [115].

Table E: Further comparisons for LLE and DR. (a) RAMiT-*slimLLE* is still better than URetinex-Net. (b) We outperform MPRNet on a benchmark dataset despite much fewer parameters.

(a) Comparison for LLE.

Method	#Params	LOL [102]		VE-LOL-cap [63]	
		PSNR	SSIM	PSNR	SSIM
URetinex-Net [104]	361K	21.33	0.8348	21.22	0.8593
RAMiT- <i>slimLLE</i> (ours)	358K	23.77	0.8379	28.38	0.8835

(b) Comparison for DR.

Method	#Params	Test100 [115]		Rain100H [106]	
		PSNR	SSIM	PSNR	SSIM
MPRNet [111]	3,637K	30.27	0.8970	30.41	0.8990
RAMiT (ours)	935K	30.44	0.9012	29.69	0.8775

## A.9 More Related Works

**CNN-based IR.** Since pioneering image restoration (IR) works, such as SRCNN [18] and DnCNN [118], outperformed traditional methods [29, 88, 89, 77, 32], many deep learning-based networks have been introduced. They were primarily based on convolutional neural networks (CNN) [17, 47, 19, 50, 58, 119, 120, 108, 44, 107]. In addition, the outstanding CNN approaches were proposed, using the residual learning [86, 49, 99, 2, 82, 53, 127, 117, 22], the

distillation-based structures [42, 41, 61], non-local priors [60, 126, 131, 76], the attention mechanisms [125, 14, 68, 79, 70, 75, 69, 54, 5, 23], or Retinex theory [103, 129, 64, 124, 104].

**Transformer-based IR.** Few years ago, Vision Transformer (ViT) [21] showed remarkable performances for image classification task, which encouraged many IR researchers to employ ViT architecture. As discussed in Sec. 2 related works of the main contents, various studies have striven to resolve the limitation of window self-attention [56, 101, 123, 10, 116, 11, 110]. In addition to them, other ViT-based IR methods have been developed. IPT [7] pre-trained ViT-based networks on the large datasets, such as ImageNet1K [15], and fine-tuned them for each IR task. DPT [96] computed vertical and horizontal angular self-attention to improve light field super-resolution performance. ESRT [67] and HNCT [24] solved super-resolution problems by utilizing composition of lightweight CNN and Transformer structures. DRT [57] adapted a plain recursive Transformer blocks to recover rainy and snowy images. Moreover, KiT [51] and DRSformer [9] constructed Transformer architectures that calculated a sparse self-attention by top- $k$  selection using  $k$ -NN algorithm, thereby enhancing various IR performances, similar to [95, 94]. Most recently, SRFormer [132] proposed a permuted self-attention using channel-wise compressed *key*, *value*.

## B Experimental Details

**In Common.** As explained in Sec. 4.1, we optimized  $L_1$  pixel-loss between  $I_{RC}$  and  $I_{HQ}$  with the Adam optimizer [48] ( $\beta_1 = 0.9, \beta_2 = 0.99, \epsilon = 10^{-8}$ ), where  $I_{RC}$  is a reconstructed image and  $I_{HQ}$  is a high-quality ground-truth image. Learning rate was initialized as  $0.0004 \times 64/\text{batch\_size}$ . The data augmentation method for LQ and HQ pairs was already specified in the main contents. Before we fed the LQ input images to the network, each input was normalized using mean and std pre-calculated from the LQ training datasets corresponding to each task. Note that since we used the random (blind) noise levels ( $\sigma$ ) for training our denoising networks, we used mean and std of HQ training datasets for color and grayscale denoising. When computing the training loss, the normalized  $I_{RC}$  was de-normalized (opposite process of normalization). For evaluation, an input image  $I_{LQ}$  was up-sized by symmetric padding to fit the size to a multiplier ( $= 32 = 8 \times 2^2$ ) of the local-window  $M(= 8)$  and downsizing number ( $= 2^2$ ) for the hierarchical stages. We implemented all processes using PyTorch and two NVIDIA GeForce RTX 4090 GPUs. The implementation details of RAMiT-1 and RAMiT are in Tab. F.

Table F: Implementation details of RAMiT and RAMiT-1. “depths” and “num heads” count the number of D-RAMiT blocks ( $\mathbb{K}_1, \mathbb{K}_2, \mathbb{K}_3, \mathbb{K}_4$ ) and multi-heads ( $L$ ) in stage 1, 2, 3, 4. Correspondingly, the setting of “chsa head ratio =25%” indicates that  $(L_{sp}, L_{ch})$  is placed as  $[(3, 1), (3, 1), (3, 1), (3, 1)]$  in each stage.

Overall Architecture	dim ( $C$ ) depths num heads chsa head ratio window size ( $M$ )	64 [6, 4, 4, 6] [4, 4, 4, 4] 25% 8	(RAMiT-1: 1) (RAMiT-1: N/A) (RAMiT-1: N/A)
Feed-Forward Network (FFN)	hidden ratio activation	2.0 GELU [34]	
MobiVari	version exp factor expand groups activation	2 1.2 4 LeakyReLU [72]	
Dropout	attention map attention project drop path	0.0 0.0 0.0	
Others	optimizer initialized learning rate learning rate decay batch size epoch / total datapoints	Adam [48] ( $\beta_1 = 0.9, \beta_2 = 0.99, \epsilon = 10^{-8}$ ) $0.0004 \times 64/\text{batch\_size}$ half (see paragraphs below) see paragraphs below 500 / 32M (SR), 400 / 10M (Others)	

**Super-Resolution.** We trained RAMiT for  $\times 2$  task from scratch, of which the training epochs were set to 500. For  $\times 3, \times 4$  tasks, we followed a warm-start strategy [59], where we fine-tuned the final reconstruction module for 50 epochs (warm-start phase) before fine-tuning whole network parameters (whole-finetuning phase) lasting for 250 epochs. In warm-start phase, the network parameters pre-trained on  $\times 2$  task were loaded to initialize  $\times 3, \times 4$  networks, except for the reconstruction module. Learning rate was decayed by half at  $\{200, 300, 400, 425, 450, 475\}$  and  $\{50, 100, 150, 175, 200, 225\}$  epochs for training from scratch ( $\times 2$ ) and whole-finetuning phase



( $\times 3, \times 4$ ), respectively. Learning rate of warm-start phase remained as a constant (*i.e.*,  $0.0004 \times 64/\text{batch\_size}$ ). We also linearly increased learning rate from 0 to  $0.0004 \times 64/\text{batch\_size}$  during the first 20 epochs of the training from scratch and whole-finetuning phase (warmup epoch [27]). Each training image was cropped into a patch size of  $64 \times 64$  with 64 batch size regardless of training from scratch or warm-start strategy. To consistently manage the datapoints per epoch, we repeated each datapoint 80 and 18.551 times for DIV2K and DF2K datasets, which made the number of training images used for an epoch equal to 64,000.

**Others.** For color and grayscale denoising, low-light enhancement, and deraining, we adapted the progressive learning [110], where the patch size was initially set to  $64 \times 64$ , and then progressively increased to  $96 \times 96$  and  $128 \times 128$  after {100, 200} epochs, respectively. The corresponding batch size was {64, 32, 16}. We decrease learning rate by half at {200, 300, 350, 375} epochs. Warmup epoch was the same as super-resolution. The training process lasted for 400 epochs. Similar to super-resolution, we repeated each datapoint 3.0, 14.006, and 1.8234 times for denoising, low-light enhancement, and deraining, respectively (about 25,000 datapoints were used per epoch). While we obtained the synthetic or real-captured low and high quality image pairs of low-light enhancement and deraining from public sources<sup>5</sup>, the Additive White Gaussian Noise (AWGN) for low quality noisy input images of denoising tasks was generated by the following PyTorch-like code:

```
AWGN = torch.randn(*img_hq.shape)* $\sigma$ /255
img_lq = img_hq + AWGN,
```

where the random seed was set to 0 for the evaluation process (in training, seed is not given to implement blind denoising); `img_lq` and `img_hq` indicate low and high quality images;  $\sigma$  is noise level set to one among [15, 25, 50] for testing or sampled uniformly between  $0 \sim 50$  for training.

## C More Visual Comparisons

In the last six pages (P. 24–29 after References) of this document, we provide additional visual comparisons of our RAMiT and other networks. These visual results exhibit the effectiveness of our approach on super-resolution (Figs. H and I), denoising (Figs. J and K), low-light enhancement (Fig. L), and deraining (Fig. M).

## D Broader Impacts

Our study on lightweight deep neural networks can assist research and application in developing countries where access to expensive equipment is limited. For example, the equipment used to capture images displayed on a cutting-edge 4K screen can be very expensive and therefore inaccessible to many, but our lightweight technology allows for the use of low-cost capture equipment to obtain ultra-high definition images. Furthermore, our research yields benefits such as reduced energy consumption and carbon emissions due to its low computational requirements. On the other hand, this work could have negative impacts such as the potential for misuse in invading people’s privacy. For instance, it could be used to restore censored materials produced for privacy protection or to enhance images captured from a distance. In addition, our novel method is definitely not perfect, which may leads to the possibility of image alteration resulting in distortion of critical information and the dissemination of inaccurate information to the public. Therefore, the proposed RAMiT can be further improved in future works.

## E Limitations

Despite achieving state-of-the-art results on five lightweight image restoration tasks, this work lacks experiments on other lightweight tasks (*e.g.*, deblurring or JPEG compression artifacts reduction). In future studies, we aim to address these problems to further demonstrate the extension power of RAMiT. Additionally, we did not investigate other lightweight techniques such as quantization [52, 93, 62, 36, 35] and pruning [45, 128, 113]. If we apply these methods to our network, the size of RAMiT can be further reduced without any significant drops in performance, making it suitable for mobile or edge devices. Considering these limitations, this work could be improved in the future.

<sup>5</sup>LOL and VE-LOL datasets can be found in this [website1](#) and this [website2](#). Deraining Testsets and Rain13K can be publicly downloaded in this [google-drive1](#) and this [google-drive2](#).

## References

- [1] Eirikur Agustsson and Radu Timofte. Ntire 2017 challenge on single image super-resolution: Dataset and study. In *Proceedings of the IEEE conference on computer vision and pattern recognition workshops*, pages 126–135, 2017.
- [2] Namhyuk Ahn, Byungkong Kang, and Kyung-Ah Sohn. Fast, accurate, and lightweight super-resolution with cascading residual network. In *Proceedings of the European conference on computer vision (ECCV)*, pages 252–268, 2018.
- [3] Pablo Arbelaez, Michael Maire, Charles Fowlkes, and Jitendra Malik. Contour detection and hierarchical image segmentation. *IEEE transactions on pattern analysis and machine intelligence*, 33(5):898–916, 2010.
- [4] Jimmy Lei Ba, Jamie Ryan Kiros, and Geoffrey E Hinton. Layer normalization. *arXiv preprint arXiv:1607.06450*, 2016.
- [5] Parichehr Behjati, Pau Rodriguez, Carles Fernández, Isabelle Hupont, Armin Mehri, and Jordi González. Single image super-resolution based on directional variance attention network. *Pattern Recognition*, 133:108997, 2023.
- [6] Marco Bevilacqua, Aline Roumy, Christine Guillemot, and Marie Line Alberi-Morel. Low-complexity single-image super-resolution based on nonnegative neighbor embedding. *BMVA press*, 2012.
- [7] Hanting Chen, Yunhe Wang, Tianyu Guo, Chang Xu, Yiping Deng, Zhenhua Liu, Siwei Ma, Chunjing Xu, Chao Xu, and Wen Gao. Pre-trained image processing transformer. In *Proceedings of the IEEE/CVF Conference on Computer Vision and Pattern Recognition*, pages 12299–12310, 2021.
- [8] Liangyu Chen, Xiaojie Chu, Xiangyu Zhang, and Jian Sun. Simple baselines for image restoration. In *Computer Vision–ECCV 2022: 17th European Conference, Tel Aviv, Israel, October 23–27, 2022, Proceedings, Part VII*, pages 17–33. Springer, 2022.
- [9] Xiang Chen, , Hao Li, Mingqiang Li, and Jinshan Pan. Learning a sparse transformer network for effective image deraining. In *Proceedings of the IEEE/CVF Conference on Computer Vision and Pattern Recognition (CVPR)*, 2023.
- [10] Zheng Chen, Yulun Zhang, Jinjin Gu, Yongbing Zhang, Linghe Kong, and Xin Yuan. Cross aggregation transformer for image restoration. In Alice H. Oh, Alekh Agarwal, Danielle Belgrave, and Kyunghyun Cho, editors, *Advances in Neural Information Processing Systems*, 2022.
- [11] Haram Choi, Jeongmin Lee, and Jihoon Yang. N-gram in swin transformers for efficient lightweight image super-resolution. In *Proceedings of the IEEE/CVF Conference on Computer Vision and Pattern Recognition*, 2023.
- [12] Haram Choi, Cheolwoong Na, Jinseop Kim, and Jihoon Yang. Exploration of lightweight single image denoising with transformers and truly fair training. In *Proceedings of the 2023 International Conference on Multimedia Retrieval*, 2023.
- [13] Taco Cohen and Max Welling. Group equivariant convolutional networks. In *International conference on machine learning*, pages 2990–2999. PMLR, 2016.
- [14] Tao Dai, Jianrui Cai, Yongbing Zhang, Shu-Tao Xia, and Lei Zhang. Second-order attention network for single image super-resolution. In *Proceedings of the IEEE/CVF conference on computer vision and pattern recognition*, pages 11065–11074, 2019.
- [15] Jia Deng, Wei Dong, Richard Socher, Li-Jia Li, Kai Li, and Li Fei-Fei. Imagenet: A large-scale hierarchical image database. In *2009 IEEE conference on computer vision and pattern recognition*, pages 248–255. Ieee, 2009.
- [16] Mingyu Ding, Bin Xiao, Noel Codella, Ping Luo, Jingdong Wang, and Lu Yuan. Davit: Dual attention vision transformers. In *Computer Vision–ECCV 2022: 17th European Conference, Tel Aviv, Israel, October 23–27, 2022, Proceedings, Part XXIV*, pages 74–92. Springer, 2022.
- [17] Chao Dong, Yubin Deng, Chen Change Loy, and Xiaoou Tang. Compression artifacts reduction by a deep convolutional network. In *Proceedings of the IEEE international conference on computer vision*, pages 576–584, 2015.
- [18] Chao Dong, Chen Change Loy, Kaiming He, and Xiaoou Tang. Image super-resolution using deep convolutional networks. *IEEE transactions on pattern analysis and machine intelligence*, 38(2):295–307, 2015.
- [19] Chao Dong, Chen Change Loy, and Xiaoou Tang. Accelerating the super-resolution convolutional neural network. In *Computer Vision–ECCV 2016: 14th European Conference, Amsterdam, The Netherlands, October 11–14, 2016, Proceedings, Part II 14*, pages 391–407. Springer, 2016.
- [20] Xiaoyi Dong, Jianmin Bao, Dongdong Chen, Weiming Zhang, Nenghai Yu, Lu Yuan, Dong Chen, and Baining Guo. Cswin transformer: A general vision transformer backbone with cross-shaped windows. In *Proceedings of the IEEE/CVF Conference on Computer Vision and Pattern Recognition*, pages 12124–12134, 2022.
- [21] Alexey Dosovitskiy, Lucas Beyer, Alexander Kolesnikov, Dirk Weissenborn, Xiaohua Zhai, Thomas Unterthiner, Mostafa Dehghani, Matthias Minderer, Georg Heigold, Sylvain Gelly, Jakob Uszkoreit, and Neil Houlsby. An image is worth 16x16 words: Transformers for image recognition at scale. In *International Conference on Learning Representations*, 2021.

- [22] Zongcai Du, Ding Liu, Jie Liu, Jie Tang, Gangshan Wu, and Lean Fu. Fast and memory-efficient network towards efficient image super-resolution. In *Proceedings of the IEEE/CVF Conference on Computer Vision and Pattern Recognition*, pages 853–862, 2022.
- [23] Saijie Fan, Wei Liang, Derui Ding, and Hui Yu. Lacn: A lightweight attention-guided convnext network for low-light image enhancement. *Engineering Applications of Artificial Intelligence*, 117:105632, 2023.
- [24] Jinsheng Fang, Hanjiang Lin, Xinyu Chen, and Kun Zeng. A hybrid network of cnn and transformer for lightweight image super-resolution. In *Proceedings of the IEEE/CVF Conference on Computer Vision and Pattern Recognition*, pages 1103–1112, 2022.
- [25] Rich Franzen. Kodak lossless true color image suite. *source: <http://r0k.us/graphics/kodak>*, 4(2), 1999.
- [26] Xueyang Fu, Jiabin Huang, Delu Zeng, Yue Huang, Xinghao Ding, and John Paisley. Removing rain from single images via a deep detail network. In *Proceedings of the IEEE conference on computer vision and pattern recognition*, pages 3855–3863, 2017.
- [27] Priya Goyal, Piotr Dollár, Ross Girshick, Pieter Noordhuis, Lukasz Wesolowski, Aapo Kyrola, Andrew Tulloch, Yangqing Jia, and Kaiming He. Accurate, large minibatch sgd: Training imagenet in 1 hour. *arXiv preprint arXiv:1706.02677*, 2017.
- [28] Jinjin Gu and Chao Dong. Interpreting super-resolution networks with local attribution maps. In *Proceedings of the IEEE/CVF Conference on Computer Vision and Pattern Recognition*, pages 9199–9208, 2021.
- [29] Shuhang Gu, Nong Sang, and Fan Ma. Fast image super resolution via local regression. In *Proceedings of the 21st International Conference on Pattern Recognition (ICPR2012)*, pages 3128–3131. IEEE, 2012.
- [30] Bharath Hariharan, Pablo Arbeláez, Ross Girshick, and Jitendra Malik. Hypercolumns for object segmentation and fine-grained localization. In *Proceedings of the IEEE conference on computer vision and pattern recognition*, pages 447–456, 2015.
- [31] Kaiming He, Xinlei Chen, Saining Xie, Yanghao Li, Piotr Dollár, and Ross Girshick. Masked autoencoders are scalable vision learners. In *Proceedings of the IEEE/CVF Conference on Computer Vision and Pattern Recognition*, pages 16000–16009, 2022.
- [32] Kaiming He, Jian Sun, and Xiaoou Tang. Single image haze removal using dark channel prior. *IEEE transactions on pattern analysis and machine intelligence*, 33(12):2341–2353, 2010.
- [33] Kaiming He, Xiangyu Zhang, Shaoqing Ren, and Jian Sun. Deep residual learning for image recognition. In *Proceedings of the IEEE conference on computer vision and pattern recognition*, pages 770–778, 2016.
- [34] Dan Hendrycks and Kevin Gimpel. Gaussian error linear units (gelus). *arXiv preprint arXiv:1606.08415*, 2016.
- [35] Cheeun Hong, Sungyong Baik, Heewon Kim, Seungjun Nah, and Kyoung Mu Lee. Cadyq: Content-aware dynamic quantization for image super-resolution. *arXiv preprint arXiv:2207.10345*, 2022.
- [36] Cheeun Hong, Heewon Kim, Sungyong Baik, Junghun Oh, and Kyoung Mu Lee. Daq: Channel-wise distribution-aware quantization for deep image super-resolution networks. In *Proceedings of the IEEE/CVF Winter Conference on Applications of Computer Vision*, pages 2675–2684, 2022.
- [37] Qibin Hou, Li Zhang, Ming-Ming Cheng, and Jiashi Feng. Strip pooling: Rethinking spatial pooling for scene parsing. In *Proceedings of the IEEE/CVF conference on computer vision and pattern recognition*, pages 4003–4012, 2020.
- [38] Andrew G Howard, Menglong Zhu, Bo Chen, Dmitry Kalenichenko, Weijun Wang, Tobias Weyand, Marco Andreetto, and Hartwig Adam. Mobilenets: Efficient convolutional neural networks for mobile vision applications. *arXiv preprint arXiv:1704.04861*, 2017.
- [39] Jie Hu, Li Shen, and Gang Sun. Squeeze-and-excitation networks. In *Proceedings of the IEEE conference on computer vision and pattern recognition*, pages 7132–7141, 2018.
- [40] Jia-Bin Huang, Abhishek Singh, and Narendra Ahuja. Single image super-resolution from transformed self-exemplars. In *Proceedings of the IEEE conference on computer vision and pattern recognition*, pages 5197–5206, 2015.
- [41] Zheng Hui, Xinbo Gao, Yunchu Yang, and Xiumei Wang. Lightweight image super-resolution with information multi-distillation network. In *Proceedings of the 27th acm international conference on multimedia*, pages 2024–2032, 2019.
- [42] Zheng Hui, Xiumei Wang, and Xinbo Gao. Fast and accurate single image super-resolution via information distillation network. In *Proceedings of the IEEE conference on computer vision and pattern recognition*, pages 723–731, 2018.
- [43] Md Amirul Islam\*, Sen Jia\*, and Neil D. B. Bruce. How much position information do convolutional neural networks encode? In *International Conference on Learning Representations*, 2020.
- [44] Kui Jiang, Zhongyuan Wang, Peng Yi, Chen Chen, Baojin Huang, Yimin Luo, Jiayi Ma, and Junjun Jiang. Multi-scale progressive fusion network for single image deraining. In *Proceedings of the IEEE/CVF conference on computer vision and pattern recognition*, pages 8346–8355, 2020.
- [45] Xinrui Jiang, Nannan Wang, Jingwei Xin, Xiaobo Xia, Xi Yang, and Xinbo Gao. Learning lightweight super-resolution networks with weight pruning. *Neural Networks*, 144:21–32, 2021.

- [46] Yifan Jiang, Xinyu Gong, Ding Liu, Yu Cheng, Chen Fang, Xiaohui Shen, Jianchao Yang, Pan Zhou, and Zhangyang Wang. Enlightengan: Deep light enhancement without paired supervision. *IEEE transactions on image processing*, 30:2340–2349, 2021.
- [47] Jiwon Kim, Jung Kwon Lee, and Kyoung Mu Lee. Accurate image super-resolution using very deep convolutional networks. In *Proceedings of the IEEE conference on computer vision and pattern recognition*, pages 1646–1654, 2016.
- [48] Diederik P Kingma and Jimmy Ba. Adam: A method for stochastic optimization. *arXiv preprint arXiv:1412.6980*, 2014.
- [49] Wei-Sheng Lai, Jia-Bin Huang, Narendra Ahuja, and Ming-Hsuan Yang. Deep laplacian pyramid networks for fast and accurate super-resolution. In *Proceedings of the IEEE conference on computer vision and pattern recognition*, pages 624–632, 2017.
- [50] Christian Ledig, Lucas Theis, Ferenc Huszár, Jose Caballero, Andrew Cunningham, Alejandro Acosta, Andrew Aitken, Alykhan Tejani, Johannes Totz, Zehan Wang, et al. Photo-realistic single image super-resolution using a generative adversarial network. In *Proceedings of the IEEE conference on computer vision and pattern recognition*, pages 4681–4690, 2017.
- [51] Hunsang Lee, Hyesong Choi, Kwanghoon Sohn, and Dongbo Min. Knn local attention for image restoration. In *Proceedings of the IEEE/CVF Conference on Computer Vision and Pattern Recognition*, pages 2139–2149, 2022.
- [52] Huixia Li, Chenqian Yan, Shaohui Lin, Xiwu Zheng, Baochang Zhang, Fan Yang, and Rongrong Ji. Pams: Quantized super-resolution via parameterized max scale. In *Computer Vision—ECCV 2020: 16th European Conference, Glasgow, UK, August 23–28, 2020, Proceedings, Part XXV 16*, pages 564–580. Springer, 2020.
- [53] Juncheng Li, Yiting Yuan, Kangfu Mei, and Faming Fang. Lightweight and accurate recursive fractal network for image super-resolution. In *Proceedings of the IEEE/CVF International Conference on Computer Vision Workshops*, pages 0–0, 2019.
- [54] Yufeng Li, Zhentao Fan, Jiyang Lu, and Xiang Chen. Tao-net: Task-adaptive operation network for image restoration and enhancement. *IEEE Signal Processing Letters*, 29:2198–2202, 2022.
- [55] Yu Li, Robby T Tan, Xiaojie Guo, Jiangbo Lu, and Michael S Brown. Rain streak removal using layer priors. In *Proceedings of the IEEE conference on computer vision and pattern recognition*, pages 2736–2744, 2016.
- [56] Jingyun Liang, Jiezhang Cao, Guolei Sun, Kai Zhang, Luc Van Gool, and Radu Timofte. Swinir: Image restoration using swin transformer. In *Proceedings of the IEEE/CVF International Conference on Computer Vision*, pages 1833–1844, 2021.
- [57] Yuanchu Liang, Saeed Anwar, and Yang Liu. Drt: A lightweight single image deraining recursive transformer. In *Proceedings of the IEEE/CVF Conference on Computer Vision and Pattern Recognition*, pages 589–598, 2022.
- [58] Bee Lim, Sanghyun Son, Heewon Kim, Seungjun Nah, and Kyoung Mu Lee. Enhanced deep residual networks for single image super-resolution. In *Proceedings of the IEEE conference on computer vision and pattern recognition workshops*, pages 136–144, 2017.
- [59] Zudi Lin, Prateek Garg, Atmadeep Banerjee, Salma Abdel Magid, Deqing Sun, Yulun Zhang, Luc Van Gool, Donglai Wei, and Hanspeter Pfister. Revisiting rcnn: Improved training for image super-resolution. *arXiv preprint arXiv:2201.11279*, 2022.
- [60] Ding Liu, Bihan Wen, Yuchen Fan, Chen Change Loy, and Thomas S Huang. Non-local recurrent network for image restoration. *Advances in neural information processing systems*, 31, 2018.
- [61] Jie Liu, Jie Tang, and Gangshan Wu. Residual feature distillation network for lightweight image super-resolution. In *European Conference on Computer Vision*, pages 41–55. Springer, 2020.
- [62] Jingyu Liu, Qiong Wang, Dunbo Zhang, and Li Shen. Super-resolution model quantized in multi-precision. *Electronics*, 10(17):2176, 2021.
- [63] Jiaying Liu, Dejia Xu, Wenhan Yang, Minhao Fan, and Haofeng Huang. Benchmarking low-light image enhancement and beyond. *International Journal of Computer Vision*, 129:1153–1184, 2021.
- [64] Risheng Liu, Long Ma, Jiao Zhang, Xin Fan, and Zhongxuan Luo. Retinex-inspired unrolling with cooperative prior architecture search for low-light image enhancement. In *Proceedings of the IEEE/CVF Conference on Computer Vision and Pattern Recognition*, pages 10561–10570, 2021.
- [65] Ze Liu, Han Hu, Yutong Lin, Zhuliang Yao, Zhenda Xie, Yixuan Wei, Jia Ning, Yue Cao, Zheng Zhang, Li Dong, et al. Swin transformer v2: Scaling up capacity and resolution. In *Proceedings of the IEEE/CVF Conference on Computer Vision and Pattern Recognition*, pages 12009–12019, 2022.
- [66] Ze Liu, Yutong Lin, Yue Cao, Han Hu, Yixuan Wei, Zheng Zhang, Stephen Lin, and Baining Guo. Swin transformer: Hierarchical vision transformer using shifted windows. In *Proceedings of the IEEE/CVF International Conference on Computer Vision*, pages 10012–10022, 2021.
- [67] Zhisheng Lu, Juncheng Li, Hong Liu, Chaoyan Huang, Linlin Zhang, and Tieyong Zeng. Transformer for single image super-resolution. In *Proceedings of the IEEE/CVF Conference on Computer Vision and Pattern Recognition (CVPR) Workshops*, pages 457–466, June 2022.



- [68] Xiaotong Luo, Yuan Xie, Yulun Zhang, Yanyun Qu, Cuihua Li, and Yun Fu. Latticenet: Towards lightweight image super-resolution with lattice block. In *European Conference on Computer Vision*, pages 272–289. Springer, 2020.
- [69] Feifan Lv, Yu Li, and Feng Lu. Attention guided low-light image enhancement with a large scale low-light simulation dataset. *International Journal of Computer Vision*, 129(7):2175–2193, 2021.
- [70] Hailong Ma, Xiangxiang Chu, and Bo Zhang. Accurate and efficient single image super-resolution with matrix channel attention network. In *Proceedings of the Asian Conference on Computer Vision*, 2020.
- [71] Kede Ma, Zhengfang Duanmu, Qingbo Wu, Zhou Wang, Hongwei Yong, Hongliang Li, and Lei Zhang. Waterloo exploration database: New challenges for image quality assessment models. *IEEE Transactions on Image Processing*, 26(2):1004–1016, 2016.
- [72] Andrew L Maas, Awni Y Hannun, Andrew Y Ng, et al. Rectifier nonlinearities improve neural network acoustic models. In *Proc. icml*, volume 30, page 3. Atlanta, Georgia, USA, 2013.
- [73] David Martin, Charless Fowlkes, Doron Tal, and Jitendra Malik. A database of human segmented natural images and its application to evaluating segmentation algorithms and measuring ecological statistics. In *Proceedings Eighth IEEE International Conference on Computer Vision. ICCV 2001*, volume 2, pages 416–423. IEEE, 2001.
- [74] Yusuke Matsui, Kota Ito, Yuji Aramaki, Azuma Fujimoto, Toru Ogawa, Toshihiko Yamasaki, and Kiyoharu Aizawa. Sketch-based manga retrieval using manga109 dataset. *Multimedia Tools and Applications*, 76(20):21811–21838, 2017.
- [75] Armin Mehri, Parichehr B Ardakani, and Angel D Sappa. Mprnet: Multi-path residual network for lightweight image super resolution. In *Proceedings of the IEEE/CVF Winter Conference on Applications of Computer Vision*, pages 2704–2713, 2021.
- [76] Yiqun Mei, Yuchen Fan, and Yuqian Zhou. Image super-resolution with non-local sparse attention. In *Proceedings of the IEEE/CVF Conference on Computer Vision and Pattern Recognition*, pages 3517–3526, 2021.
- [77] Tomer Michaeli and Michal Irani. Nonparametric blind super-resolution. In *Proceedings of the IEEE International Conference on Computer Vision*, pages 945–952, 2013.
- [78] Vinod Nair and Geoffrey E Hinton. Rectified linear units improve restricted boltzmann machines. In *Proceedings of the 27th international conference on machine learning (ICML-10)*, pages 807–814, 2010.
- [79] Ben Niu, Weilei Wen, Wenqi Ren, Xiangde Zhang, Lianping Yang, Shuzhen Wang, Kaihao Zhang, Xiaochun Cao, and Haifeng Shen. Single image super-resolution via a holistic attention network. In *European conference on computer vision*, pages 191–207. Springer, 2020.
- [80] Zia-ur Rahman, Daniel J Jobson, and Glenn A Woodell. Retinex processing for automatic image enhancement. *Journal of Electronic imaging*, 13(1):100–110, 2004.
- [81] Prajit Ramachandran, Barret Zoph, and Quoc V Le. Searching for activation functions. *arXiv preprint arXiv:1710.05941*, 2017.
- [82] Dongwei Ren, Wangmeng Zuo, Qinghua Hu, Pengfei Zhu, and Deyu Meng. Progressive image deraining networks: A better and simpler baseline. In *Proceedings of the IEEE/CVF conference on computer vision and pattern recognition*, pages 3937–3946, 2019.
- [83] Mark Sandler, Andrew Howard, Menglong Zhu, Andrey Zhmoginov, and Liang-Chieh Chen. Mobilenetv2: Inverted residuals and linear bottlenecks. In *Proceedings of the IEEE conference on computer vision and pattern recognition*, pages 4510–4520, 2018.
- [84] Peter Shaw, Jakob Uszkoreit, and Ashish Vaswani. Self-attention with relative position representations. In *Proceedings of the 2018 Conference of the North American Chapter of the Association for Computational Linguistics: Human Language Technologies, Volume 2 (Short Papers)*, pages 464–468, New Orleans, Louisiana, June 2018. Association for Computational Linguistics.
- [85] Wenzhe Shi, Jose Caballero, Ferenc Huszár, Johannes Totz, Andrew P Aitken, Rob Bishop, Daniel Rueckert, and Zehan Wang. Real-time single image and video super-resolution using an efficient sub-pixel convolutional neural network. In *Proceedings of the IEEE conference on computer vision and pattern recognition*, pages 1874–1883, 2016.
- [86] Ying Tai, Jian Yang, and Xiaoming Liu. Image super-resolution via deep recursive residual network. In *Proceedings of the IEEE conference on computer vision and pattern recognition*, pages 3147–3155, 2017.
- [87] Radu Timofte, Eirikur Agustsson, Luc Van Gool, Ming-Hsuan Yang, and Lei Zhang. Ntire 2017 challenge on single image super-resolution: Methods and results. In *Proceedings of the IEEE conference on computer vision and pattern recognition workshops*, pages 114–125, 2017.
- [88] Radu Timofte, Vincent De Smet, and Luc Van Gool. Anchored neighborhood regression for fast example-based super-resolution. In *Proceedings of the IEEE international conference on computer vision*, pages 1920–1927, 2013.
- [89] Radu Timofte, Vincent De Smet, and Luc Van Gool. A+: Adjusted anchored neighborhood regression for fast super-resolution. In *Computer Vision—ACCV 2014: 12th Asian Conference on Computer Vision, Singapore, Singapore, November 1-5, 2014, Revised Selected Papers, Part IV 12*, pages 111–126. Springer, 2015.

- [90] Zhengzhong Tu, Hossein Talebi, Han Zhang, Feng Yang, Peyman Milanfar, Alan Bovik, and Yinxiao Li. Maxim: Multi-axis mlp for image processing. In *Proceedings of the IEEE/CVF Conference on Computer Vision and Pattern Recognition*, pages 5769–5780, 2022.
- [91] Zhengzhong Tu, Hossein Talebi, Han Zhang, Feng Yang, Peyman Milanfar, Alan Bovik, and Yinxiao Li. Maxvit: Multi-axis vision transformer. In *Computer Vision–ECCV 2022: 17th European Conference, Tel Aviv, Israel, October 23–27, 2022, Proceedings, Part XXIV*, pages 459–479. Springer, 2022.
- [92] Ashish Vaswani, Noam Shazeer, Niki Parmar, Jakob Uszkoreit, Llion Jones, Aidan N Gomez, Łukasz Kaiser, and Illia Polosukhin. Attention is all you need. *Advances in neural information processing systems*, 30, 2017.
- [93] Hu Wang, Peng Chen, Bohan Zhuang, and Chunhua Shen. Fully quantized image super-resolution networks. In *Proceedings of the 29th ACM International Conference on Multimedia*, pages 639–647, 2021.
- [94] Haochen Wang, Jiayi Shen, Yongtuo Liu, Yan Gao, and Efstratios Gavves. Nformer: Robust person re-identification with neighbor transformer. In *Proceedings of the IEEE/CVF Conference on Computer Vision and Pattern Recognition*, pages 7297–7307, 2022.
- [95] Pichao Wang, Xue Wang, Fan Wang, Ming Lin, Shuning Chang, Hao Li, and Rong Jin. Kvt: k-nn attention for boosting vision transformers. In *Computer Vision–ECCV 2022: 17th European Conference, Tel Aviv, Israel, October 23–27, 2022, Proceedings, Part XXIV*, pages 285–302. Springer, 2022.
- [96] Shunzhou Wang, Tianfei Zhou, Yao Lu, and Huijun Di. Detail-preserving transformer for light field image super-resolution. In *Proceedings of the AAAI Conference on Artificial Intelligence*, 2022.
- [97] Tao Wang, Guangpin Tao, Wanglong Lu, Kaihao Zhang, Wenhan Luo, Xiaoqin Zhang, and Tong Lu. Restoring vision in hazy weather with hierarchical contrastive learning. *arXiv preprint arXiv:2212.11473*, 2022.
- [98] Wenxiao Wang, Lu Yao, Long Chen, Binbin Lin, Deng Cai, Xiaofei He, and Wei Liu. Crossformer: A versatile vision transformer hinging on cross-scale attention. In *International Conference on Learning Representations, ICLR*, 2022.
- [99] Xintao Wang, Ke Yu, Shixiang Wu, Jinjin Gu, Yihao Liu, Chao Dong, Yu Qiao, and Chen Change Loy. Esrgan: Enhanced super-resolution generative adversarial networks. In *Proceedings of the European conference on computer vision (ECCV) workshops*, pages 0–0, 2018.
- [100] Zhou Wang, Alan C Bovik, Hamid R Sheikh, and Eero P Simoncelli. Image quality assessment: from error visibility to structural similarity. *IEEE transactions on image processing*, 13(4):600–612, 2004.
- [101] Zhendong Wang, Xiaodong Cun, Jianmin Bao, Wengang Zhou, Jianzhuang Liu, and Houqiang Li. Uformer: A general u-shaped transformer for image restoration. In *Proceedings of the IEEE/CVF Conference on Computer Vision and Pattern Recognition*, pages 17683–17693, 2022.
- [102] Chen Wei, Wenjing Wang, Wenhan Yang, and Jiaying Liu. Deep retinex decomposition for low-light enhancement. In *British Machine Vision Conference*, 2018.
- [103] Chen Wei, Wenjing Wang, Wenhan Yang, and Jiaying Liu. Deep retinex decomposition for low-light enhancement. *arXiv preprint arXiv:1808.04560*, 2018.
- [104] Wenhui Wu, Jian Weng, Pingping Zhang, Xu Wang, Wenhan Yang, and Jianmin Jiang. Uretinex-net: Retinex-based deep unfolding network for low-light image enhancement. In *Proceedings of the IEEE/CVF Conference on Computer Vision and Pattern Recognition*, pages 5901–5910, 2022.
- [105] Jianwei Yang, Chunyuan Li, Pengchuan Zhang, Xiyang Dai, Bin Xiao, Lu Yuan, and Jianfeng Gao. Focal attention for long-range interactions in vision transformers. In A. Beygelzimer, Y. Dauphin, P. Liang, and J. Wortman Vaughan, editors, *Advances in Neural Information Processing Systems*, 2021.
- [106] Wenhan Yang, Robby T Tan, Jiashi Feng, Jiaying Liu, Zongming Guo, and Shuicheng Yan. Deep joint rain detection and removal from a single image. In *Proceedings of the IEEE conference on computer vision and pattern recognition*, pages 1357–1366, 2017.
- [107] Wenhan Yang, Shiqi Wang, Yuming Fang, Yue Wang, and Jiaying Liu. From fidelity to perceptual quality: A semi-supervised approach for low-light image enhancement. In *Proceedings of the IEEE/CVF conference on computer vision and pattern recognition*, pages 3063–3072, 2020.
- [108] Rajeev Yasarla and Vishal M Patel. Uncertainty guided multi-scale residual learning-using a cycle spinning cnn for single image de-raining. In *Proceedings of the IEEE/CVF conference on computer vision and pattern recognition*, pages 8405–8414, 2019.
- [109] Qihang Yu, Yingda Xia, Yutong Bai, Yongyi Lu, Alan L Yuille, and Wei Shen. Glance-and-gaze vision transformer. *Advances in Neural Information Processing Systems*, 34:12992–13003, 2021.
- [110] Syed Waqas Zamir, Aditya Arora, Salman Khan, Munawar Hayat, Fahad Shahbaz Khan, and Ming-Hsuan Yang. Restormer: Efficient transformer for high-resolution image restoration. In *CVPR*, 2022.
- [111] Syed Waqas Zamir, Aditya Arora, Salman Khan, Munawar Hayat, Fahad Shahbaz Khan, Ming-Hsuan Yang, and Ling Shao. Multi-stage progressive image restoration. In *CVPR*, 2021.
- [112] Roman Zeyde, Michael Elad, and Matan Protter. On single image scale-up using sparse-representations. In *International conference on curves and surfaces*, pages 711–730. Springer, 2010.
- [113] Zheng Zhan, Yifan Gong, Pu Zhao, Geng Yuan, Wei Niu, Yushu Wu, Tianyun Zhang, Malith Jayaweera, David Kaeli, Bin Ren, et al. Achieving on-mobile real-time super-resolution with neural architecture and

- pruning search. In *Proceedings of the IEEE/CVF International Conference on Computer Vision*, pages 4821–4831, 2021.
- [114] He Zhang and Vishal M Patel. Density-aware single image de-raining using a multi-stream dense network. In *Proceedings of the IEEE conference on computer vision and pattern recognition*, pages 695–704, 2018.
  - [115] He Zhang, Vishwanath Sindagi, and Vishal M Patel. Image de-raining using a conditional generative adversarial network. *IEEE transactions on circuits and systems for video technology*, 30(11):3943–3956, 2019.
  - [116] Jiale Zhang, Yulun Zhang, Jinjin Gu, Yongbing Zhang, Linghe Kong, and Xin Yuan. Accurate image restoration with attention retractable transformer. In *The Eleventh International Conference on Learning Representations*, 2023.
  - [117] Kai Zhang, Yawei Li, Wangmeng Zuo, Lei Zhang, Luc Van Gool, and Radu Timofte. Plug-and-play image restoration with deep denoiser prior. *IEEE Transactions on Pattern Analysis and Machine Intelligence*, 44(10):6360–6376, 2021.
  - [118] Kai Zhang, Wangmeng Zuo, Yunjin Chen, Deyu Meng, and Lei Zhang. Beyond a gaussian denoiser: Residual learning of deep cnn for image denoising. *IEEE transactions on image processing*, 26(7):3142–3155, 2017.
  - [119] Kai Zhang, Wangmeng Zuo, Shuhang Gu, and Lei Zhang. Learning deep cnn denoiser prior for image restoration. In *Proceedings of the IEEE conference on computer vision and pattern recognition*, pages 3929–3938, 2017.
  - [120] Kai Zhang, Wangmeng Zuo, and Lei Zhang. Ffdnet: Toward a fast and flexible solution for cnn-based image denoising. *IEEE Transactions on Image Processing*, 27(9):4608–4622, 2018.
  - [121] Lei Zhang, Xiaolin Wu, Antoni Buades, and Xin Li. Color demosaicking by local directional interpolation and nonlocal adaptive thresholding. *Journal of Electronic imaging*, 20(2):023016, 2011.
  - [122] Qiming Zhang, Yufei Xu, Jing Zhang, and Dacheng Tao. Vsa: learning varied-size window attention in vision transformers. In *Computer Vision—ECCV 2022: 17th European Conference, Tel Aviv, Israel, October 23–27, 2022, Proceedings, Part XXV*, pages 466–483. Springer, 2022.
  - [123] Xindong Zhang, Hui Zeng, Shi Guo, and Lei Zhang. Efficient long-range attention network for image super-resolution. In *European Conference on Computer Vision*, 2022.
  - [124] Yonghua Zhang, Xiaojie Guo, Jiayi Ma, Wei Liu, and Jiawan Zhang. Beyond brightening low-light images. *International Journal of Computer Vision*, 129:1013–1037, 2021.
  - [125] Yulun Zhang, Kunpeng Li, Kai Li, Lichen Wang, Bineng Zhong, and Yun Fu. Image super-resolution using very deep residual channel attention networks. In *Proceedings of the European conference on computer vision (ECCV)*, pages 286–301, 2018.
  - [126] Yulun Zhang, Kunpeng Li, Kai Li, Bineng Zhong, and Yun Fu. Residual non-local attention networks for image restoration. *arXiv preprint arXiv:1903.10082*, 2019.
  - [127] Yulun Zhang, Yapeng Tian, Yu Kong, Bineng Zhong, and Yun Fu. Residual dense network for image restoration. *IEEE Transactions on Pattern Analysis and Machine Intelligence*, 43(7):2480–2495, 2020.
  - [128] Yulun Zhang, Huan Wang, Can Qin, and Yun Fu. Learning efficient image super-resolution networks via structure-regularized pruning. In *International Conference on Learning Representations*, 2021.
  - [129] Yonghua Zhang, Jiawan Zhang, and Xiaojie Guo. Kindling the darkness: A practical low-light image enhancer. In *Proceedings of the 27th ACM international conference on multimedia*, pages 1632–1640, 2019.
  - [130] Yuzhi Zhao, Lai-Man Po, Qiong Yan, Wei Liu, and Tingyu Lin. Hierarchical regression network for spectral reconstruction from rgb images. In *Proceedings of the IEEE/CVF Conference on Computer Vision and Pattern Recognition Workshops*, pages 422–423, 2020.
  - [131] Shangchen Zhou, Jiawei Zhang, Wangmeng Zuo, and Chen Change Loy. Cross-scale internal graph neural network for image super-resolution. *Advances in neural information processing systems*, 33:3499–3509, 2020.
  - [132] Yupeng Zhou, Zhen Li, Chun-Le Guo, Song Bai, Ming-Ming Cheng, and Qibin Hou. Srformer: Permuted self-attention for single image super-resolution. *arXiv preprint arXiv:2303.09735*, 2023.

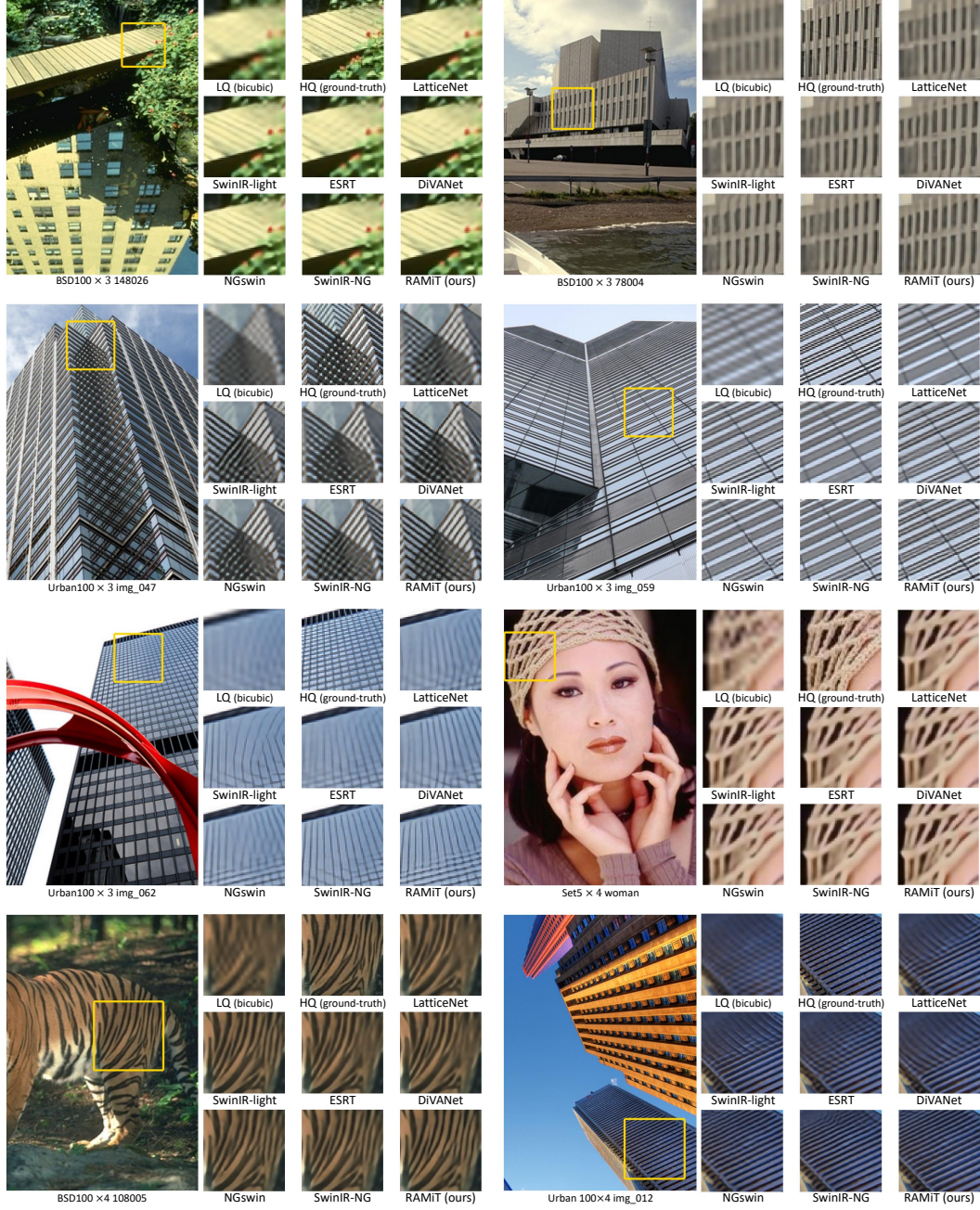
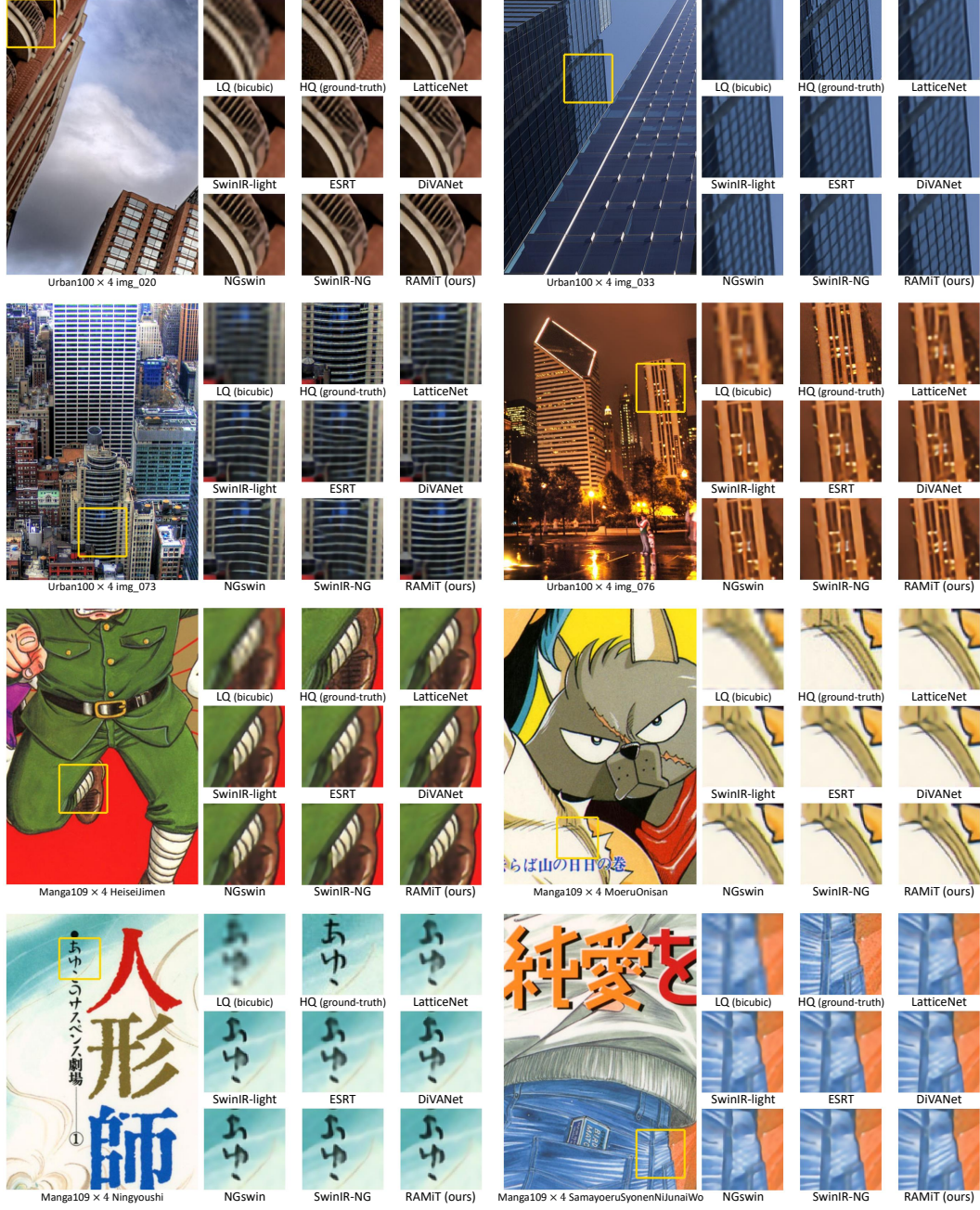


Figure H: Visual comparisons of super-resolution. LQ: Low-Quality input. HQ: High-Quality target.





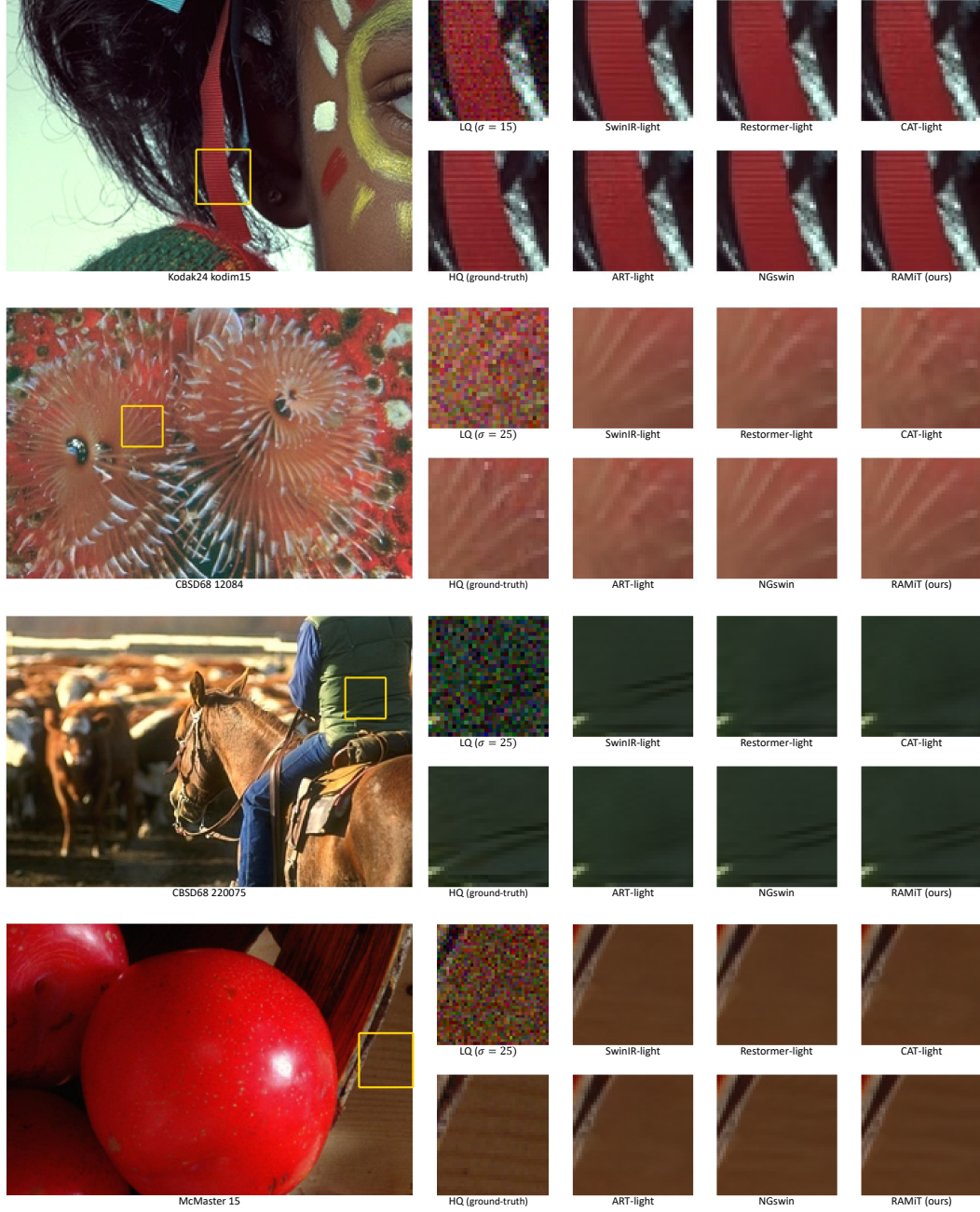


Figure J: Visual comparisons of denoising. LQ: Low-Quality input. HQ: High-Quality target.



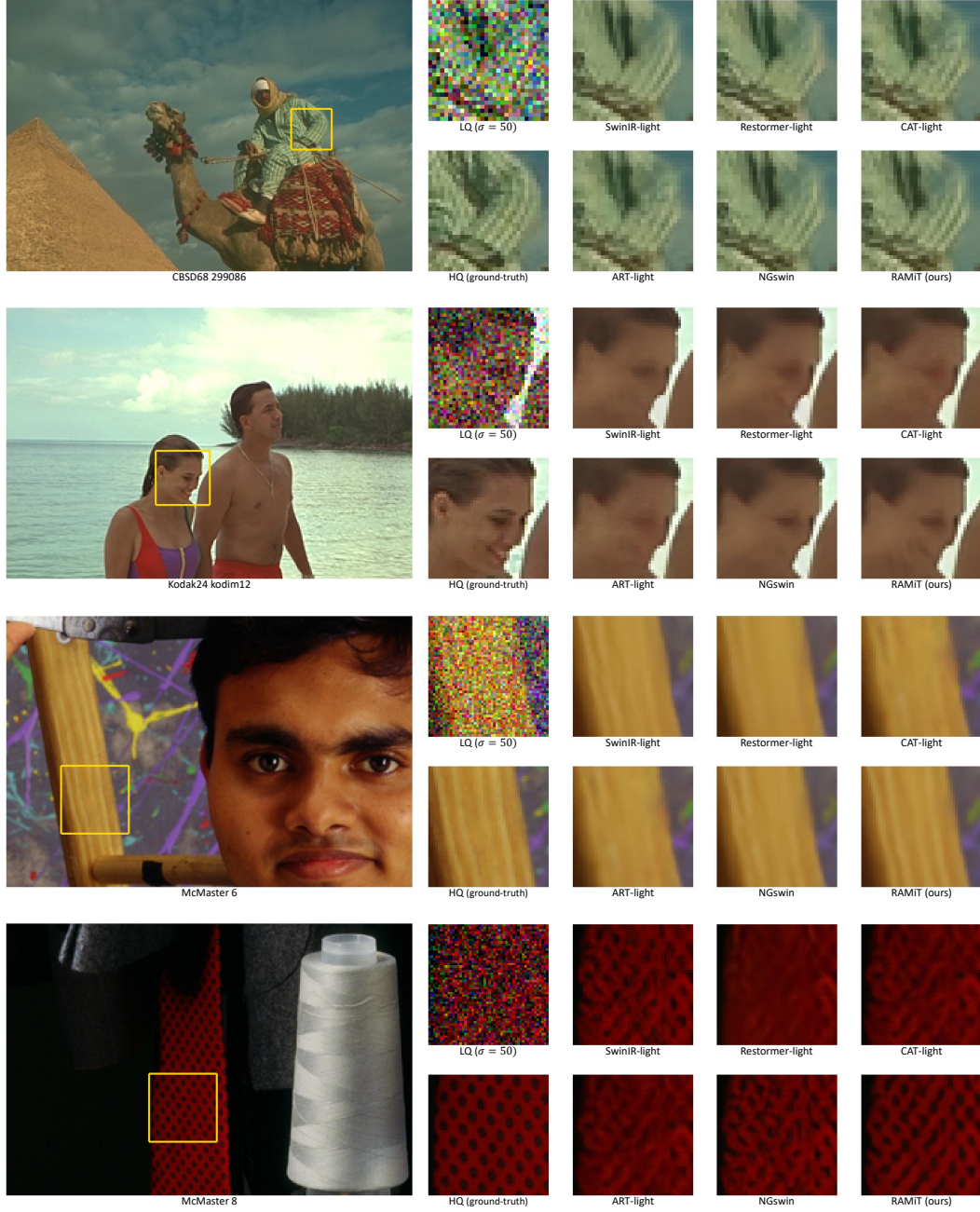


Figure K: Visual comparisons of denoising. LQ: Low-Quality input. HQ: High-Quality target.



Figure L: Visual comparisons of low-light enhancement. LQ: Low-Quality input. HQ: High-Quality target.



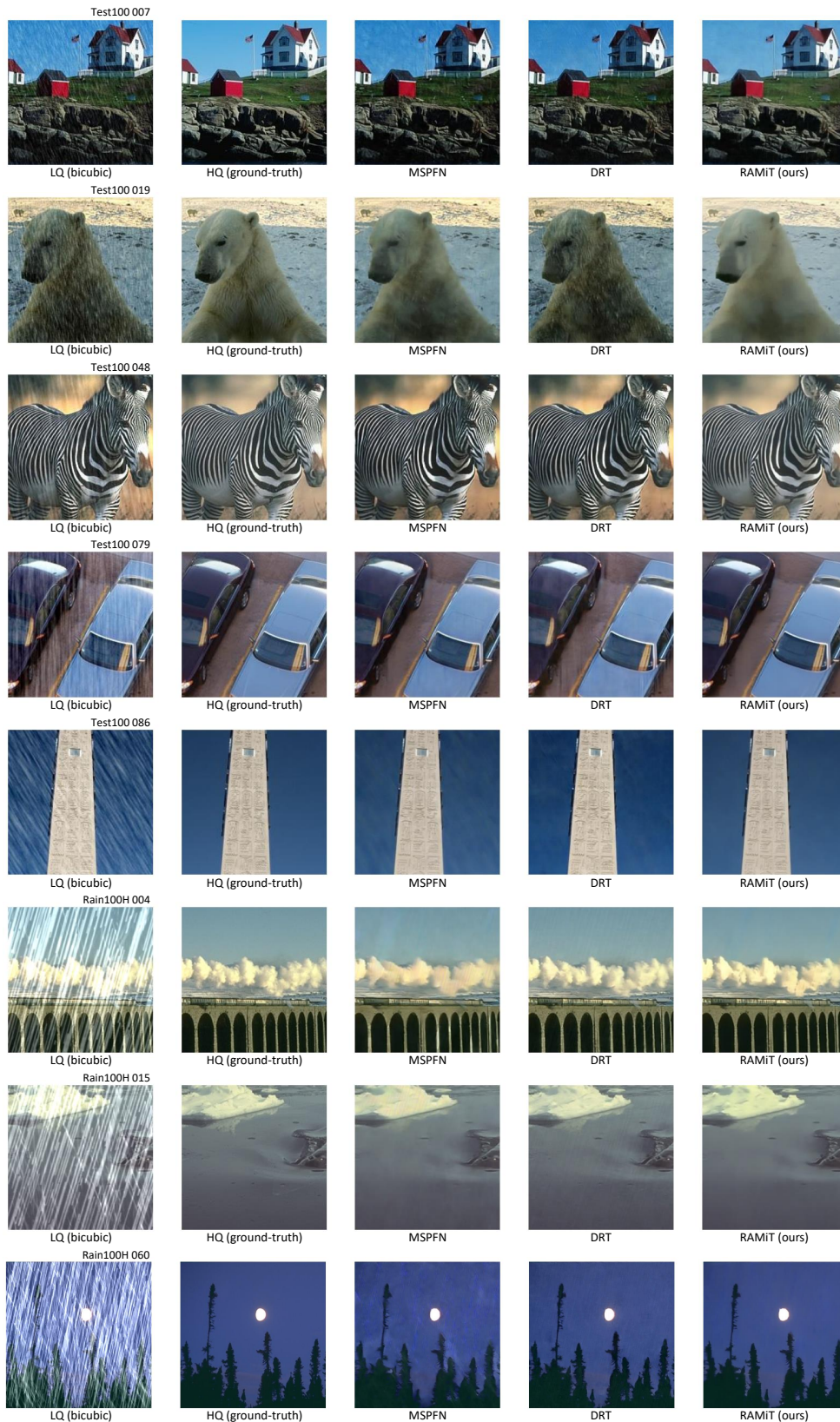


Figure M: Visual comparisons of deraining. LQ: Low-Quality input. HQ: High-Quality target.